May 2020

Calcium Selective Polymeric Contrast Agents

Christian Cole Nguyen
Clemson University, colenguyen3@gmail.com

CALCIUM SELECTIVE POLYMERIC CONTRAST AGENTS

A Thesis
Presented to
the Graduate School of
Clemson University

In Partial Fulfillment
of the Requirements for the Degree
Master of Science
Materials Science and Engineering

---

by
Christian Nguyen
May 2020

Accepted by:
Dr. Olin Mefford, Committee Chair
Dr. Mark Bolding
Dr. Igor Luzinov
Dr. Stephen Foulger

ABSTRACT

This work employs organic and polymer synthesis to construct a novel polymeric contrast agent for the application of mild traumatic brain injury in which affects so many lives not only in the united states by also internationally as well. Our approach to tackling this issue is to take advantage of diffuse axial injury and the phenomena of the fluctuation of free calcium ions after trauma occurs. We aim to take advantage of chelation chemistry. For this, we carefully construct a polymeric contrast agent that contains free carboxylic acid groups that can alternate between coordinating with gadolinium species in our contrast agent and the free calcium ions. In this way, what is hopefully obtained is an ion response polymeric contrast agent that can be for medical imaging purposes.

The first proposed idea of our work involves simple free radical polymerization containing carboxylic acids on the backbone of the polymer and a conjugated chelating component, which is vastly like ProHance(gadoteridol) a commercially available contrast agent. The polymer contrast agents were then successfully characterized using nuclear magnetic resonance (NMR) and Fourier transform inferred spectroscopy (FTIR) for structural analysis. Furthermore, magnetic resonance imaging (MRI) imagining properties determined using a 3 T coil, and the result were recorded and analyzed. While in later works, a more know calcium chelator 1,2 bis(aminophenoxy)ethane-N, N, N’, N’-tetraacetic acid (BAPTA) is latter introduced as well as more advanced synthetic techniques in hopes better to improve the first design of the original concept.

ACKNOWLEDGMENTS

First, I would like to acknowledge Dr. Thompson Mefford for giving me this opportunity, and working for him has been a pleasure. Followed by my group members who have been helpful throughout this process. Then I would like to take the time to acknowledge Eric Zhang and the Foulger group as well as Kim Ivey for allowing me to use their instrumentation. Furthermore, I would like to recognize the Brooks Sports Science Foundation for providing the funding necessary to do this work. I would also like to thank Dr. Bolding and Ryan Willoughby at the University of Alabama, Birmingham, for staying late on some nights and running so many of our samples. Lastly, I would like to take the time to thank my friends and family, especially my grandparents, for their support during this process. Without them, this would not be possible.

TABLE OF CONTENTS

Page

LIST OF TABLES

Table Page

LIST OF FIGURES

CHAPTER ONE

Introduction and review of literature

1.1 Principals of magnetic resonance imaging

Magnetic resonance imaging (MRI) has emerged as one of the most versatile medical imaging techniques, providing a pathway for non-evasive imaging techniques. In essence, it takes advantage of the hydrogen nucleus due to the high natural abundance of the H^1 of 99.9844% and deuterium 0.0156% (1). MRI is a great practical application for fundamental principles. When water protons in the body are introduced to a magnetitic field, the magnetic dipole of the protons align in the direction of the magnetic field, as shown in figure 1.1 (2).

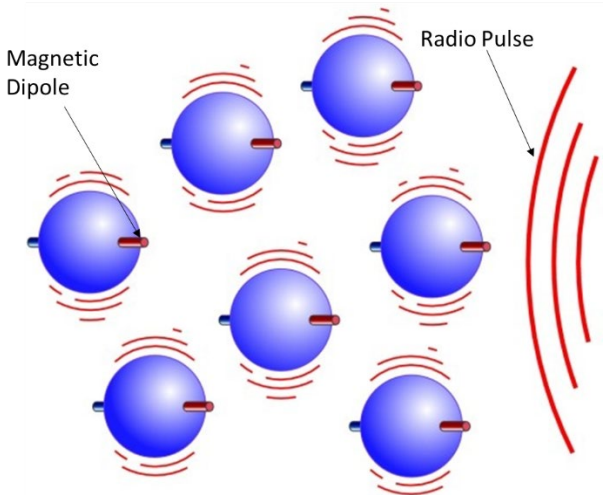

Figure 1.1) Alignment of atomic nuclei by magnetic field then applied radio pulse (2).

The radio pulse also, shown in figure 1.1, affect the equilibrium position of the protons, which gives rise to two different types of relaxation mechanisms, spin-lattice

(T_1) and spin-spin relaxation(T_2). T_1 is the equilibration of the net magnetization from the direction of the magnetic field, as shown in figure 1.2. T_2 is the dephasing of the magnetic vector along the X-Y plane perpendicular to the course of the magnetic field.

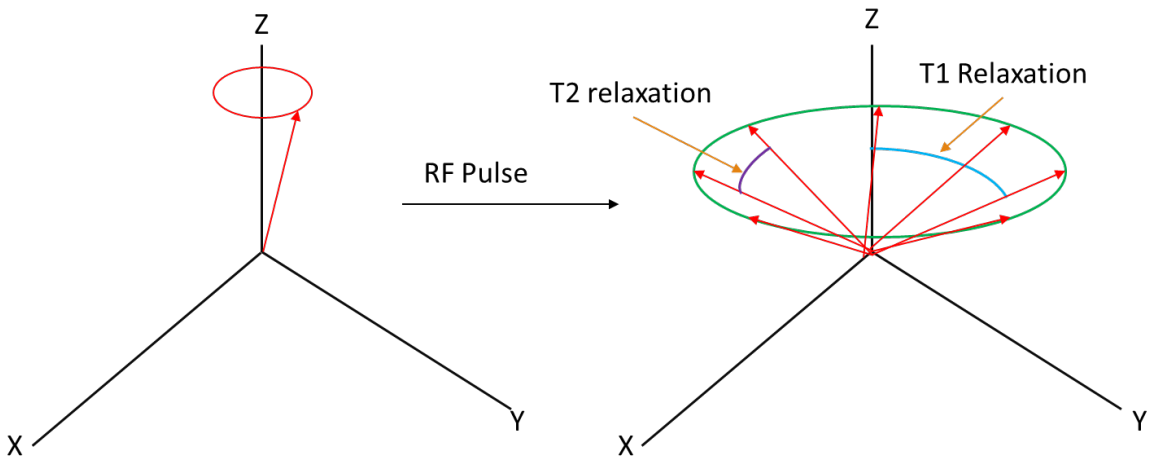

Figure 1.2) Schematic of both T_1 and T_2 relaxation mechanisms

Systemic radio pulse sequences by changing Inversion recovery (IR) times and reputation time (TR) sequences generate T_1 and T_2 maps. In most cases for T_1, a range of IR times is picked, followed by a constant short TR on the vary from 1-5 seconds by keeping the TR short it limits the T_2 interaction. For T_2 measurements, a series of echo time(TE's) are picked, followed by a long TR to show T_2 interactions (3). Moreover, T_1 and T_2 relaxation vary from the environment. For example, the cerebral spinal fluid will have a different T_1 and T_2 as opposed to the white or grey matter in the brain.

1.2 MRI contrast agents

The development of contrast agents enhanced MRI resolution, MRI contrast agents are widely used to enhance T_1 or T_2 times. Typically, gadolinium-based chelates are used T_1 contrast in clinics (4). The reason for this is that gadolinium consists of seven unpaired electrons in the outer shell of the metal ion giving rise to its unique magnetic properties. However, T_2 typically uses iron oxide nanoparticles because they disrupt the magnetic field locally, causing inhomogeneities in the applied magnetic field flux and influencing T_2 the relaxation mechanism(5). The T_1 mechanism works with the interaction of the water protons with either the inner or outer sphere diameter forcing the relaxation of the water proton.

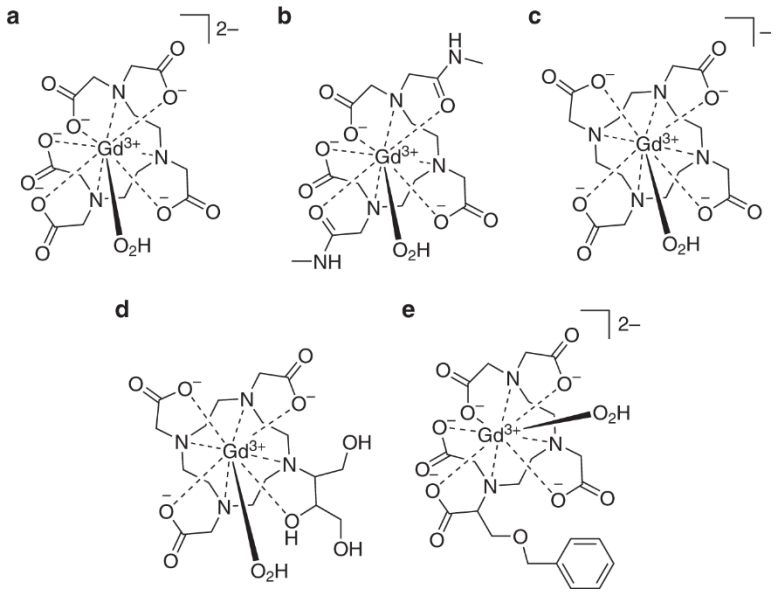

Figure 1.3) Schematic of gadolinium chelate interaction with water(6).

Moreover, this chelation is not stationary; water molecules constantly move in and out of the inner and outer spheres, thus making the metal complex and proton interaction a dynamic process. In most common contrast agents, approximately 60% of the interaction is from the inner sphere, while the other 40% is contributed to the outer sphere(7). Either T_1 or T_2 contrast work in such a way to reduce T_1 times or T_2 times, thus providing a contrast on T_1 or T_2 weighted images, respectively. Furthermore, the T_1 and T_2 can be calculated based on paramagnetic ion shown in equation 1. Where $T_{1,\,obs}$ is the observed relaxation time, $T_{1,d}$ is the relaxation time of background, R_1 is the relaxation rate of contrast agent and finally [Gd] is the concentration of gadolinium

$$\frac{1}{T_{1,\mathrm{obs}}} = \frac{1}{T_{1,\mathrm{d}}} + r_1\,[\mathrm{Gd}] \qquad \text{(Equation 1.1)}$$

Equation 1.1 demonstrates that there is a linear relationship between the concentration of gadolinium and the observe relaxation time. Certain contrast agents already approved for clinical use have their values well defined, such as Gadovist(gadobutrol), which has a relxativity of both R_1 and R_2 of about 3.5 and 4.0, respectively. The relxativity of the contrast agent is not only dependent on the ligand of the metal ion, but also on the field strength that is applied**.** In general, the relxativity constant r_1 decreases as field strength goes up(8, 9). Furthermore, this is predominantly because of the shift in the Larmor frequency, which is proportional to the magnetic field(4, 10, 11). More recently, since the success of Food drug

administration (FDA) approved contrast agents. Attention has turned to the use of contrast agents to target specific physiological events in the body, such as (Na^+, K^+, Mg^{2+}, and Ca^{2+}) (12).

Trade Name or Internal Code	0.47 T†		1.5 T		3 T		4.7 T	
	r_1	r_2	r_1	r_2	r_1	r_2	r_1	r_2
MAGNEVIST	3.4 (3.2–3.6)	4.0 (3.8–4.2)	3.3 (3.1–3.5)	3.9 (2.8–5.0)	3.1 (2.8–3.4)	3.7 (3.4–4.0)	3.2 (3.0–3.4)	4.0 (3.8–4.2)
GADOVIST	3.7 (3.5–3.9)	5.1 (4.8–5.4)	3.3 (3.1–3.5)	3.9 (3.1–4.7)	3.2 (2.9–3.5)	3.9 (3.6–4.2)	3.2 (3.0–3.4)	3.9 (3.7–4.1)
PROHANCE	3.1 (2.9–3.3)	3.7 (3.5–3.9)	2.9 (2.7–3.1)	3.2 (2.5–3.9)	2.8 (2.6–3.0)	3.4 (3.1–3.7)	2.8 (2.7–2.9)	3.7 (3.5–3.9)
MULTIHANCE	4.2 (3.9–4.4)	4.8 (4.6–5.0)	4.0 (3.8–4.2)	4.3 (3.8–4.8)	4.0 (3.7–4.3)	4.7 (4.4–5.0)	4.0 (3.8–4.2)	5.0 (4.7–5.3)
DOTAREM	3.4 (3.2–3.6)	4.1 (3.9–4.3)	2.9 (2.7–3.1)	3.2 (2.5–3.9)	2.8 (2.6–3.0)	3.3 (3.0–3.6)	2.8 (2.7–2.9)	3.7 (3.5–3.9)
OMNISCAN	3.5 (3.3–3.7)	3.8 (3.6–4.0)	3.3 (3.1–3.5)	3.6 (3.0–4.2)	3.2 (2.9–3.5)	3.8 (3.5–4.1)	3.3 (3.1–3.5)	4.1 (3.9–4.3)
TESLASCAN	1.9 (1.8–2.0)	2.1 (2.0–2.2)	1.6 (1.5–1.7)	2.1 (1.4–2.8)	1.5 (1.3–1.7)	2.3 (2.0–2.6)	1.6 (1.5–1.7)	2.7 (2.6–2.8)
OPTIMARK	4.2 (4.0–4.4)	5.2 (4.9–5.5)	3.8 (3.6–4.0)	4.2 (3.5–4.9)	3.6 (3.3–3.9)	4.5 (4.2–4.8)	3.8 (3.6–4.0)	4.7 (4.5–4.9)
RESOVIST	20.6 (19.5–21.7)	86 (82–90)	8.7 (8.2–9.2)	61 (54–68)	4.6 (4.3–4.9)	143 (132–154)	2.8 (2.7–2.9)	176 (167–185)
FERIDEX/ ENDOREM	27 (26–28)	152 (144–160)	4.7 (4.4–5.0)	41 (39–43)	4.1 (3.8–4.4)	93 (87–99)	2.3 (2.2–2.4)	105 (100–110)
Gadomer	16.5 (15.7–17.3)	17 (16–18)	17.3 (16.4–18.2)	22 (21–23)	13.0 (12.3–13.7)	23 (22–24)	9.1 (8.6–9.6)	22 (21–23)
MS-325	5.8 (5.5–6.1)	6.7 (6.4–7.0)	5.2 (4.9–5.5)	5.9 (5.3–6.5)	5.3 (5.0–5.6)	6.1 (5.7–6.5)	5.5 (5.2–5.8)	6.9 (6.5–7.3)
PRIMOVIST	5.3 (5.0–5.6)	6.2 (5.9–6.5)	4.7 (4.5–4.9)	5.1 (4.5–5.7)	4.3 (4.0–4.6)	5.5 (5.2–5.8)	4.9 (4.7–5.1)	6.3 (6.0–6.6)
SH U 555 C	23.9 (22.7–25.1)	54 (51–57)	13.2 (12.5–13.9)	44 (41–47)	7.3 (6.9–7.7)	57 (54–60)	4.3 (4.1–4.5)	66 (63–69)

*Values in L $mmol^{-1}$ s^{-1}.
†Measured at 40°C (see text for details).

Table 1.1) Table of different relaxivities at different magnetic fields and different contrast agents. (13)

1.3 Traumatic Brain Injury (TBI) and the physiological importance of calcium

In recent years TBI has been a growing concern, with the majority TBI on sports-related brain injuries. Yearly, about 2.5 million people in the United States are affected by TBI, along with 75 to 90 % of theses TBI injuries to be mild traumatic brain injuries (14). Moreover, there is not an adequate way to successfully diagnose or quantify the trauma the brain has received; instead, the treatment relies on the symptoms displayed by the subject. Testing mTBI is subjective and that this often causes miss diagnoses. Moreover, this leads to a degree of uncertainty in the severity of the

trauma(15). Calcium plays an essential role in brain injury as well as other neurological events and diseases. Fluctuations of calcium levels in the brain after trauma causes elevated levels of calcium in the intercellular and lowering calcium levels in the extracellular region (16). The phenomenon(diffuse axel injury) of the transport from calcium from the extracellular region of the brain to the intracellular region, where there is stretching and tearing of the axonal neurons(17). Furthermore, changes from calcium homeostasis can also have an impact on memory loss and other neurological dysfunctions(18). Studies indicate that current calcium levels existing in the extracellular region is in the range of about 0.1 mM to about 1.2 mM for what is considered proper calcium homeostasis (19). Moreover, the range of normal intracellular calcium levels is on the order of about 50 to 100 nM (20)**.** Therefore, the level of calcium levels between both the intercellular region and extracellular region varies significantly, causing a high gradient between them. Approximately the extracellular region is about 10000 times more. Providing that at the time of injury, there is significant diffusion between the two regions, which in the end causes neurological cell death. As calcium levels flood the intracellular region, the is a measurable drop in the extracellular region after trauma was induced (18). Thus, a contrast agent that can detect changes in calcium is essential for the nature of this phenomenon. As mentioned above, calcium is vital for neurological events. As described in this study but also in other physiological areas as well, such as the heart. Ideally, it becomes the goal of this work to be able to generate contrast agents with

known material properties, quantification of certain psychological events. Helping to improve the lives of patients as well as further an understanding of the human body as well.

1.4 Ion sensing contrast agents

Ion sensing contrast agents are growing in development with the promise that they will help target specific ions that change during neurological events. A few of these novel contrast agents are still currently under construction. For example, a contrast agent that proved sensitive to zinc selectivity is presently being developed (21).

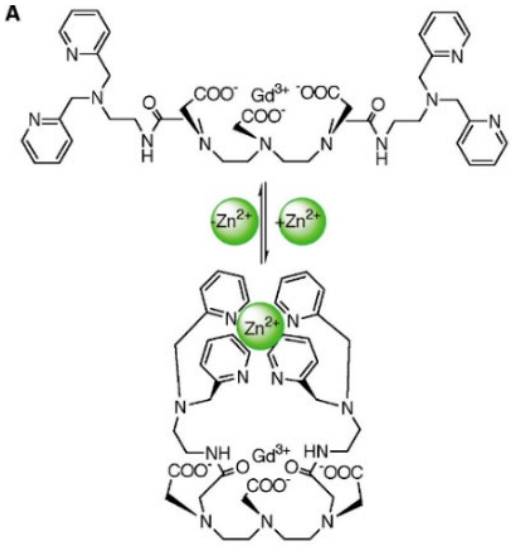

Figure 1.4) Gadolinium coordinatized complex showing association and dissociation equilibrium with the presence of zinc ions. (21)

In which they have developed an organic molecule that was then further chelated to gadolinium. Figure 1.4 displays the structural conformation that occurs, then zinc is introduced into the system and thus changing the relaxivity of the contrast agent. Indicating that this complex then demonstrated a high affinity for Zn ions(21).

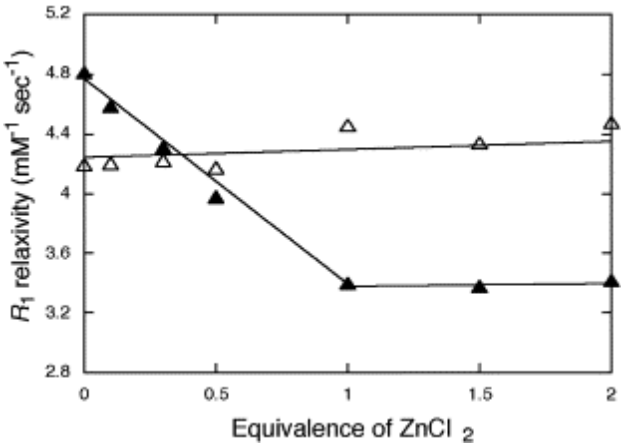

Figure 1.5) Graph of equivalence of $ZnCl_2$ as a function of relaxivity. (21)

The plot of the R1 vs. $ZnCl_2$ graph that demonstrates change indicating a dependence on zinc ions, as shown in figure 1.5. The graph shows that as the amount of $ZnCl_2$, the relaxivity starts to decrease until it begins to plateau off at one equivalent of $ZnCl_2$.The graph indicates a change in relaxivity until one molar ratio. Furthermore, other contrast agents in development show a dependence on calcium showed a calcium dependence using calmodulin and iron oxide nanoparticles(22). Thus, predominately

making it a T_2 contrast agent instead of T_1. However, the calmodulin showed a dependence of around 500 μM(22).

Furthermore, one of the more recent developments was the use and modification of 1,2 bis(aminophenoxy)ethane-N, N, N', N'-tetraacetic acid (BAPTA) as a way to synthesis a contrast agent that is effective and sensitive to calcium ions (23). As mentioned in the article, they successfully produced a manganese contrast agent that demonstrated a high affinity to calcium ions. They created the contrast agent by taking BAPTA and modifying it through nitration then a reduction to put a secondary amine successfully. Moreover**,** in figure 1.6, this gadolinium complex demonstrates its selectivity of Ca^{+2} over Mg^{2+} ions, which is one of the competing ions that is also a presence in the brain. The plot described in figure 1.6 displays relaxivity vs. a metal concentration (Mg^{+2}or Ca^{+2}). The two curves suggest that contrast dye is more efficient with the addition of calcium over magnesium, showing a change in relaxivity as the concentration of metal ions change. It is indicating about a 25% change in relaxivity at peak concentrations of metal ion levels. The contrast agent created could be used as a potential method to detect calcium in the brain.

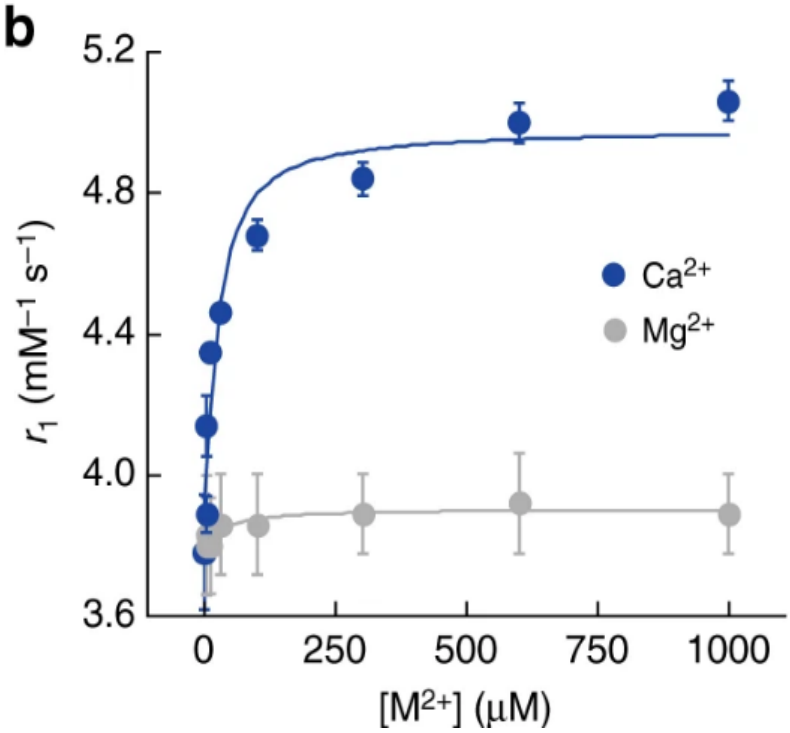

Figure 1.6) Graph of relaxivity of changes as a function of calcium and magnesium free ions (21)

This idea of ion growing contrast agents is growing, and it is one of the goals of this work to expand this idea of ions sensitive contrast agents to incorporate polymers instead of just small molecules.

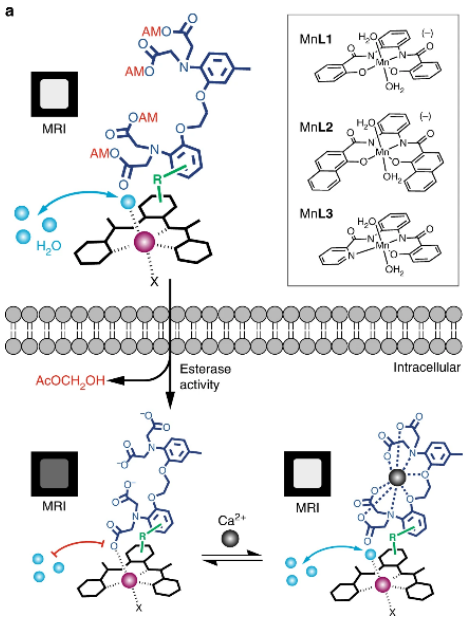

Figure 1.7) Figure showing Calcium interaction with BAPTA conjugated MRI contrast structure (21)

More interestingly, if we make a comparison of carboxylic acid ratios, we can try to understand what is happening with the carboxylic acid and calcium interaction. In a theoretical scenario, it would take one free calcium ion per 2 carboxylic acid giving a max ratio of 0.5 [Ca]/[COOH]. When the ratio of [Ca]/[COOH] was examined in Angelovski et al., work his macromolecule seemed to demonstrate that the shortest T_1 time being around 2 [Ca]/[polymer concentration] or about 1 [Ca]/[COOH] (24). Looking back at other literature examples such as the publication of the work of a Barandov et al. showed his macromolecules has a [Ca]/[COOH] of around 1 to 1.5 both demonstrating where the onset where his relaxivity curve starts to behave asymptotically (25).

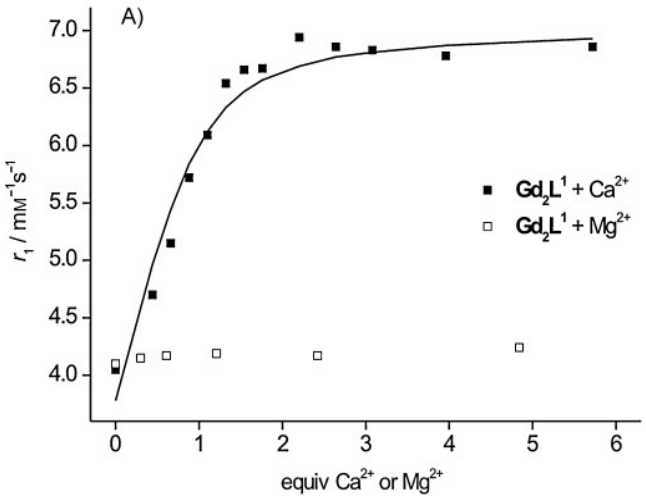

Figure 1.8) graph showing calcium interaction with BAPTA conjugated MRI contrast structure (22)

1.5 Fundamentals of chelation chemistry

An understanding of chelation chemistry is necessary for the creation of these contrast agents. When examining chelates, there are three aspects the central metal atom, the chelating molecules, and the nature of the interaction between the chelating molecules and the central metal species. First, the metal ion forms complex bonds to its neighboring atoms allowing acceptance from an electron pair and allowing it to create a metal-ligand bond (26). This interaction with neighboring atoms attributes to the solubility of the metal ion and a reduction in toxicity from the metal ion(27).

Moreover, it is this interaction that allows contrast agents to become possible. For example, gadolinium in its free ion form is extremely toxic; however, in typical FDA approved contrast agents, the predominate chelator to this is some derivative of diethylenetriamine pentaacetic acid (DTPA). This chelation mechanism dramatically reduces the toxicity to the human body but taking up coronating sites that could interact with biological matter (28). Calcium chelators has been an interest in this work for the described in 1.3. One of the first calcium chelators is ethylene glycol-bis (β-aminoethyl ether)-N, N, N', N'-tetraacetic acid (EGTA). However, it had some limitations, such as the kinetics of calcium bindings and the sensitivity to pH. To address some of the issues that EGTA had, a chemical company named Tsien developed BAPTA, which showed much high selectivity of magnesium, lower pH sensitivity, and higher rates of calcium association and dissociation (29).

Most literature displayed shows four carboxylic acids from calcium-sensitive chelators. Perhaps this is likely due to a combination of more chelation elements and the structural conformation in space that can cause the orientation of compound to arrange itself around the metal species. In this way, the organics molecule acts as a change keeping the inorganic component at the center of the compound.

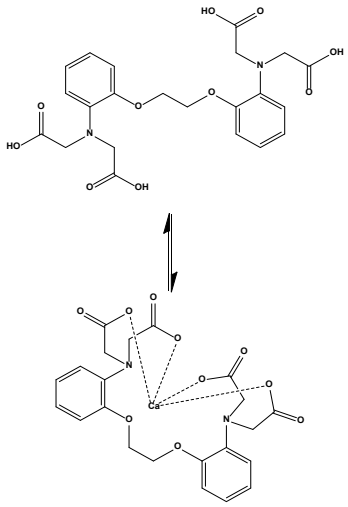

Figure 1.9) calcium interaction dye interaction with BAPTA dye

Its the kinetics moderates the effectiveness of chelation. The faster the associates and dissociation of calcium, the more effective the chelator is. Essentially the higher the equilibrium constant in equation 2 means that the [calcium-ligand] concentration is higher, thus favoring metal-ligand complex coordination over the presence of free calcium. Equation 2 defines the chelation strength of the organic compound to the free calcium. Where K is the equilibrium constant and [calcium-ligand] is the concentration of calcium bound to the ligand, [free-calcium] is the Ca^{+2} ions in solution and [ligand] is the concentration of unbound ligands.

$$\mathrm{K} = [\text{calcium-ligand}]/[\text{free-calcium}][\text{ligand}] \text{ (equation 1.2)}$$

Furthermore, this constant is greatly dependent on the pH of the system. This work focuses on gadolinium-based contrast agents because of the unique magnetic properties described in 1.2. Gadolinium chelates typically has a coordination number

of 9, such as Gd (III)Cl_3 hexahydrate, gadobutrol, and gadoteridol. In gadobutrol and gadoteridol, there are eight coordinating ligands with an open available coordinating site for water interaction. This limits biological interaction while keeping the metal ion species soluble in polar media.

1.6 Objectives

It is the goal of this work to build off previous knowledge and construct an ion-sensitive polymer MRI contrast agent using the knowledge of organic and polymer chemistry. Many of these polymeric reactions in the following chapters are either free radical polymerization or ionic reactions. With simple organic reactions such as SN2 reactions or click reactions. As well as extensive characterization techniques. Such as nuclear magnetic resonance (NMR), Fourier transmission inferred spectroscopy (FTIR), and Inductively coupled plasma mass spectrometry (ICP-MS). NMR after every step of synthesis with the addition of FTIR for certain steps. Then the final product gadolinium concentration was then tested using ICP-MS. As stated, before the primary goal of this project is to create a polymeric contrast agent that could potentially detect free calcium ions. Also, this aims to discuss the effect of molecular weight on the relaxivity, T_1, and T_2 relaxation times of the polymeric contrast agent. To approach the problem, we first started with a simple approach, which described in chapter 2. Following a more advanced and controlled synthesis with the use of an already pre-established calcium-sensing chelator (BAPTA -AM), which is then conjugated on to a polymer backbone, which described in detail in chapter 3.

CHAPTER 2

Synthesis and characterization of Gd- 1,4,7,10-tetraazacyclododecane-1,4,7-tris (acetic acid) ethyl vinyl ether co maleic anhydride and analysis of MRI properties

2.1 Introduction

This chapter introduces one of the first approaches to create a polymeric MRI contrast agent. In this work, a simple method was adopted. It was thought that if it was possible to simplify the problem by constituting the polymeric contrast agent in two parts. A "chelating" component and a calcium responsive component. Moreover, the product that was needed to be synthesized had to a have at least readily accessible carboxylic acid components to bind to the free calcium in the system. As well as the ability to modify the polymer backbone as well. For this approach, we needed to select the monomers carefully. Furthermore, the polymer that we needed to create also had the constraint of being an alternating copolymer so that each carboxylic acid on the polymer backbone could coordinate with the corresponding gadolinium ion. Conveniently there is one well-known polymer that can fit this category. An alternating copolymer between vinyl ethers and maleic anhydride is known to produce alternating copolymer (30, 31). For the monomer selection, 2-chloroethyl vinyl ether and maleic anhydride were chosen as the monomers. 2-chloroethyl vinyl ether is chosen because the vinyl chlorine group will provide a means of functionalization to cognate the chelating molecule. Once the molecule was chosen, the next decision is to pick a chelator component that we then could couple with the polymer. The chelator should be modeled after already approved

contrast agents such as Gadovist (gadobutrol) and ProHance (gadoteridol). This will allow us to compare it to a known reference. This chapter will discuss the synthesis of this polymeric contrast agent along with chemical, structural characterization, and its potential use as an MRI contrast agent. Ultimately a chemical structure of the corresponding polymer shown in figure 2.1 was chosen, and its possible interaction with calcium will take place. As calcium comes into proximity to the polymer backbone, the carboxylic acid will interact with calcium over coordinating with the gadolinium opening two free water interaction sites. Effectively making it a calcium-sensing polymeric contrast agent.

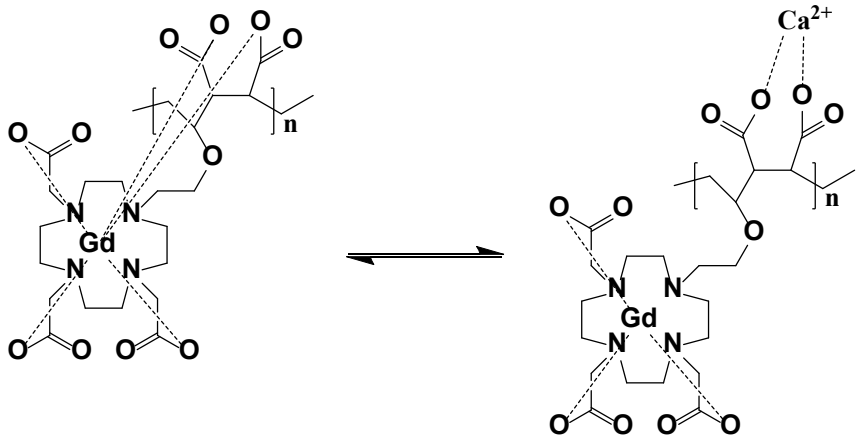

Figure 2.1) Theoretical interaction with calcium and polymeric contrast agent with the carboxylic acid group on the polymer backbone.

2.2 Synthesis of 1,4,7-tris(*tert*-butoxycarbonylmethyl)-1,4,7,10-tetraazacyclododecane) (PDO3A)

The synthesis of PDO3A was followed following Jagardish et al. As shown in figure 2.2. First, the cyclen(1,4,7,10-tetraazacyclododecane) was put into suspension with ten equivalents of sodium acetate with dimethylacetamide (DMA) under an inert N_2 atmosphere. Then three equivalents of t-butyl bromoacetate were dissolved in DMA. Afterward, the cyclen sodium acetate suspension was then cooled down to -20 °C in an acetone bath. Then the t-butyl bromoacetate solution was then added dropwise over 5 minutes in which then the solution was then allowed to reach room temperature and continued stirring overnight. After 24 hours of stirring, water was then added into the solution until a clear solution was observed with any solids that were then was filtered out.

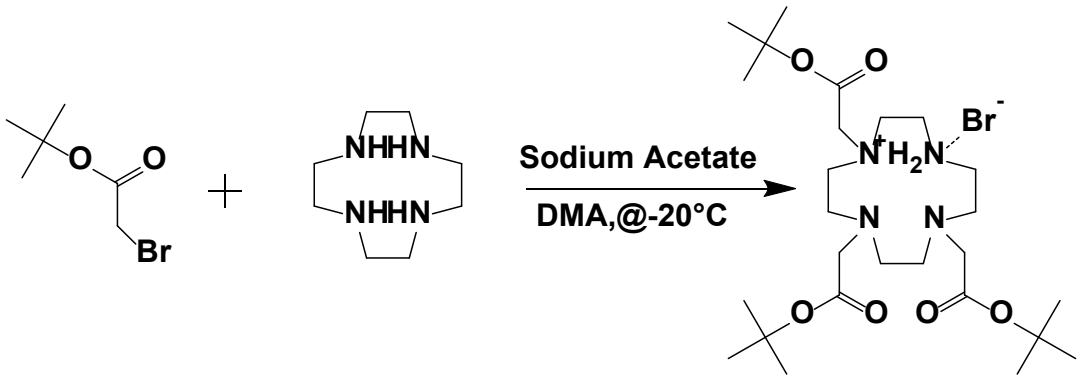

Figure 2.2) Trialkylation of t-butyl bromoacetate with cyclen for the formation of ,4,7-tris(tert-butoxycarbonylmethyl)-1,4,7,10-tetraazacyclododecane) hydro-bromine.

The product was then extracted from the solution by adding sodium bicarbonate until the crude product precipitated out of solution, which then was collected through vacuum filtration. The crude product was then dissolved in chloroform and washed 3x with water then dried with magnesium sulfate. The magnesium sulfate was then removed through filtration, and the organic solution was reduced under vacuum before precipitating out the cleaned product with the addition of diethyl ether. The product was then collected after filtration. The product was then purified using silica gel chromatography with a mobile phase of 10:1 dichloromethane (DCM) and methanol solution. The solution was made by taking 500 ml of DCM and adding 50 ml of methanol. Silica gel was then added to a glass chromatography column. The amount of silica was based on 20x the mass of the crude product that was going to be purified. The first step was to put the silica into a slurry with the DCM-methanol solution. After then it was added to the column. The about 1 column's worth of DCM-methanol solution was then added with gently tapping the

sides of the column to ensure compact packing. Afterward, just enough DCM-methanol solution mixture was added to dissolve the crude product. It was then pipetted into the column and allowed to dissipate through the silica. In which fractions were taken every 10 to 15 ml. The fractions were checked using an iodine stain on a TLC plate to examine the product's elution time. After the fractions were collected, each was reduced under vacuum, and an NMR was taken of each fraction. After examining the NMR of each fraction, the purist fraction was collected and combined, which yielded the NMR spectra in figure 2.3. The peaks corresponding at 1.4 are significant of the t-butyl esters, while the peaks at 2.5 to 3.2 correlate to the cyclic ring, and the peaks 3.4 to 3.7 pertain to the protons on the t-butyl ester arm located next to the nitrogen. Given the proton NMR was able to identify each peak after purification is adequate proof that the reaction was successful. Furthermore, the NMR proton chemical shifts are also consistent with the literature values of the corresponding compound.

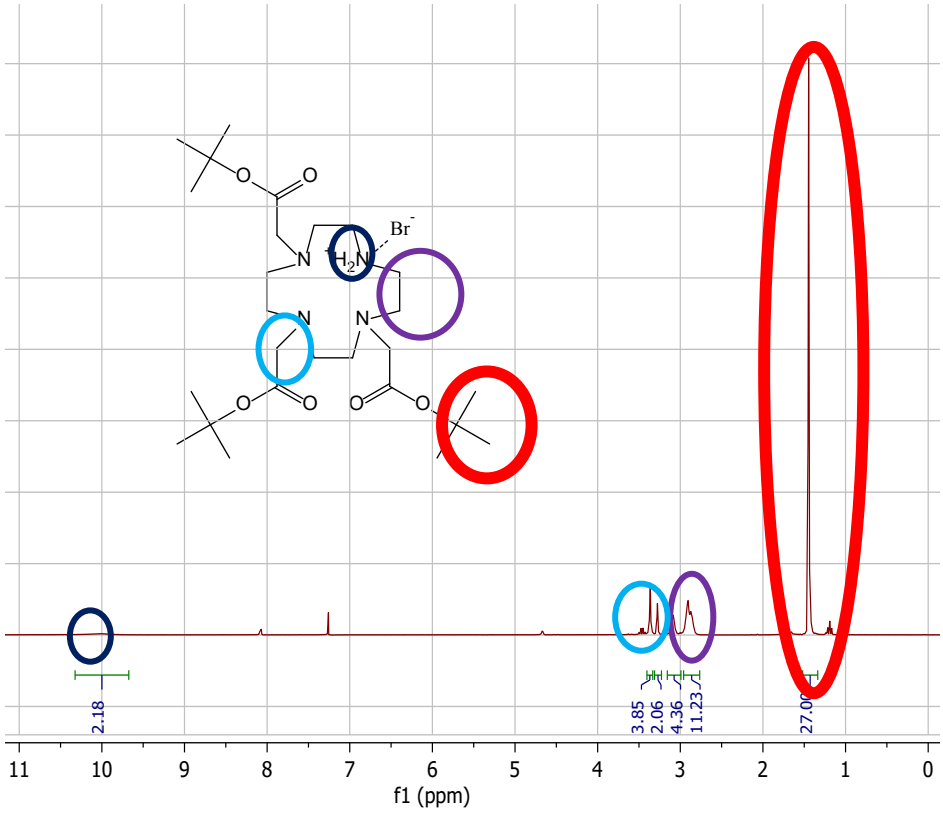

Figure 2.3) NMR of 4,7-tris(tert-butoxycarbonylmethyl)-1,4,7,10-tetraazacyclododecane) hydro-bromine.

After the POD3A salt was correctly characterized with NMR, cleavage of the HBr group was then done using potassium bicarbonate in anhydrous acetonitrile with a temperature of 50℃ as described in Xiao Y, Paudel R, Liu J, Ma C, Zhang Z, Zhou S (5). Afterward, the filtration of potassium bicarbonate was done; then, the organic solution was reduced under vacuum until dry. In order to remove any residual base, it was then dissolved in chloroform and washed with 3x times with water. After this, it was dried with magnesium sulfate then reduced under vacuum to afford PDO3A, as shown in figure 2.4. The

difference between the cleaved PDO3A oil and the PDO3A salt is the reduction of the peak corresponding to 10ppm. As well as a change in physical properties, the PDO3A is just a clear, viscous oil, while the PDO3A is a white powder.

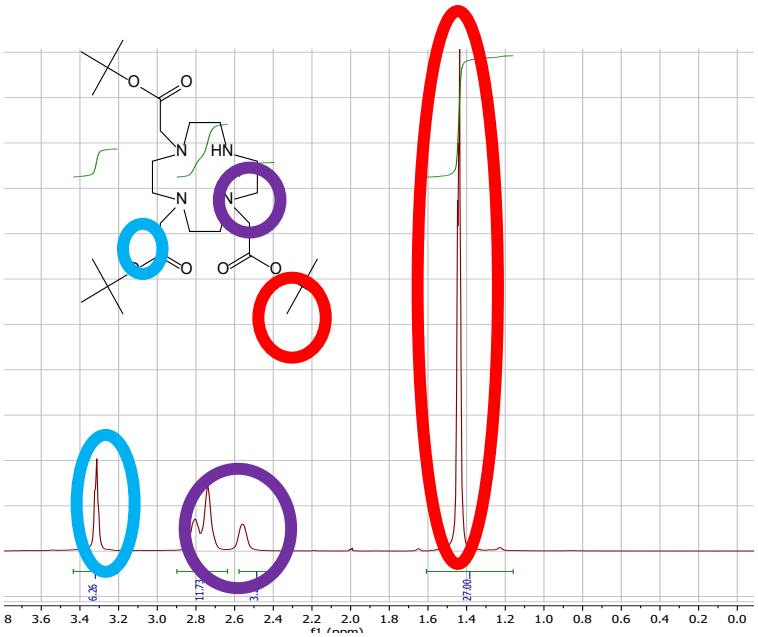

Figure 2.4) NMR of 4,7-tris(tert-butoxycarbonylmethyl)-1,4,7,10-tetraazacyclododecane)

2.3 Synthesis of chloroethyl vinyl ether co maleic anhydride

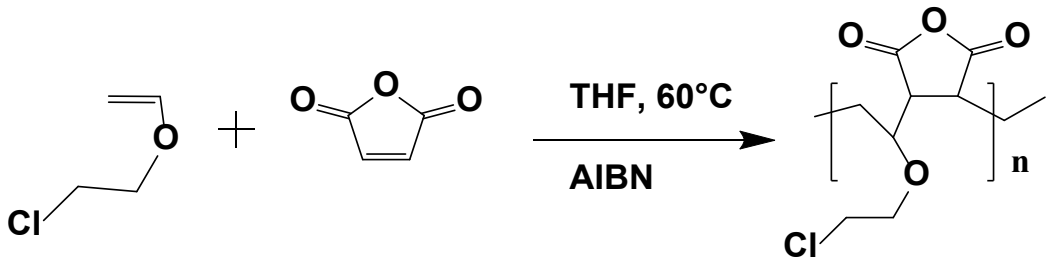

Figure 2.5) Scheme of radical polymerization of 2-chlorethylvinyl ether and maleic anhydride.

An alternating copolymerization was done between 2-chloroethyl vinyl ether and maleic anhydride, as shown in figure 2.5. The polymerization conducted as a free radical polymerization using 2,2'-Azobis(2-methylpropionitrile) (AIBN) as the radical initiator. This reaction was done in an inert environment where 1:1 molar equivalent of 2-chloroethyl vinyl ether, maleic anhydride, and AIBN were added to a flask with the addition of tetrahydrofuran (THF). The reaction was then allowed to go for 2 hours. Afterward, the solution was then reduced under pressure. Then finally, the product was precipitated the diethyl ether and collected through vacuum filtration. An NMR and FTIR were then obtained and shown in figure 2.6 and figure 2.7 respectability.

In this proton NMR, the total integration came out to be 1644 protons yielding a molecular weight of about 370 protons giving the approximate molecular weight of about 11,000 g/mol and about 72 repeat units. The molecular weight is done by normalizing the NMR peak at 1.7 ppm as the AIBN starting unit and normalizing it to 12 protons because

the termination mechanism is termination by disproportion for further structural conformation, and FTIR analysis was also done. The FTIR analysis was able to identify all functional groups in the polymer showing structural confirmation that the polymer was successfully synthesized.

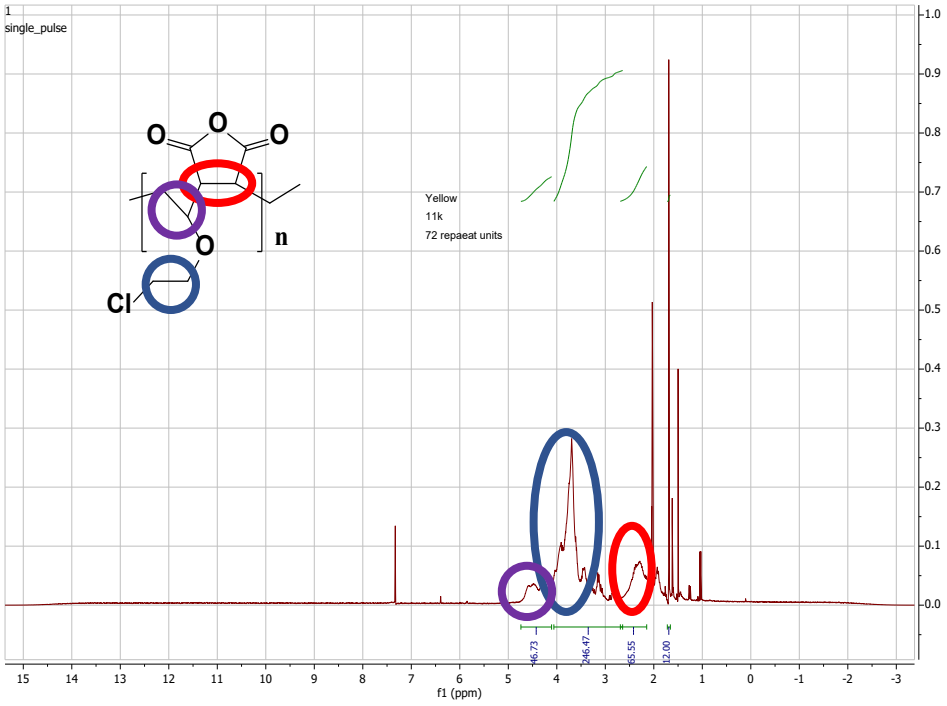

Figure 2.6) NMR of 2-chloroethylvinyl ether-co-Maleic anhydride

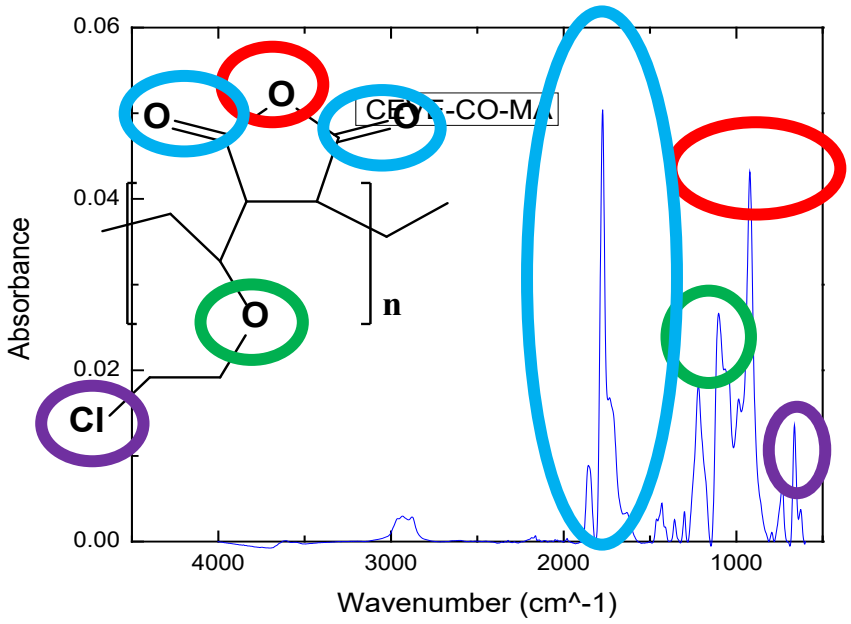

Figure 2.7) FTIR of 2-chloroethylvinyl ether-co-maleic anhydride

2.4 Synthesis of modified 1,4,7,10-tetraazacyclododecane-1,4,7-tris(*tert*-butoxycarbonylmethyl) ethyl vinyl ether co Maleic anhydride (CEVE-co-MA)

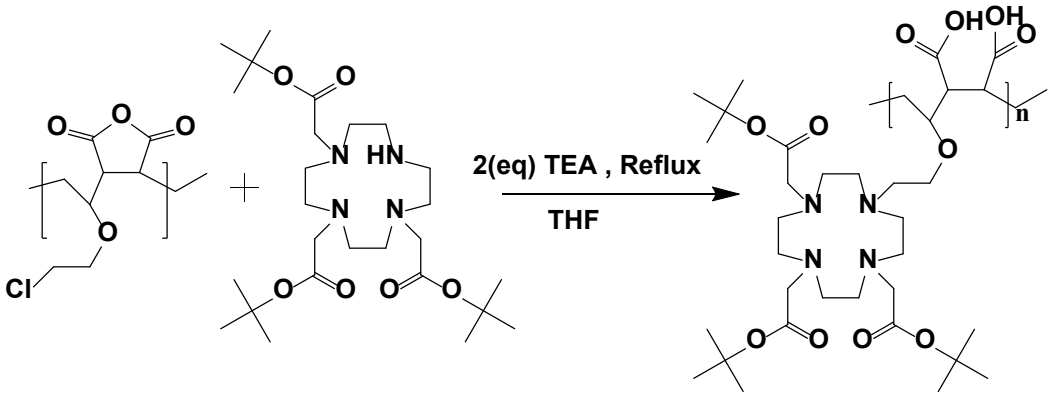

Figure 2.8) Scheme of modified 1,4,7,10-tetraazacyclododecane-1,4,7-tris(tert-butoxycarbonylmethyl) ethyl vinyl ether co maleic anhydride (CEVE-co-MA)

With the successful synthesis of both out polymer and out corresponding contrast agent, now a simple Sn2 reaction can be used to react the secondary amine on the PDO3A with the alkyl halide on the chloroethyl vinyl ether. For this, we react 1:1 molar equivalent of our alternating copolymer and the POD3A with TEA under reflux for 24 hours. The solution was then precipitated in hexane and then purified using 7.5k molecular weight dialysis tubing, after which the following NMR spectra and FTIR spectra in figure 2.9 and figure 2.10 respectively. In this particular case, the following NMR showed us the approximate molecular weights of 12,725 g/mol and was determined similarly to how the method was done in section 2.3.

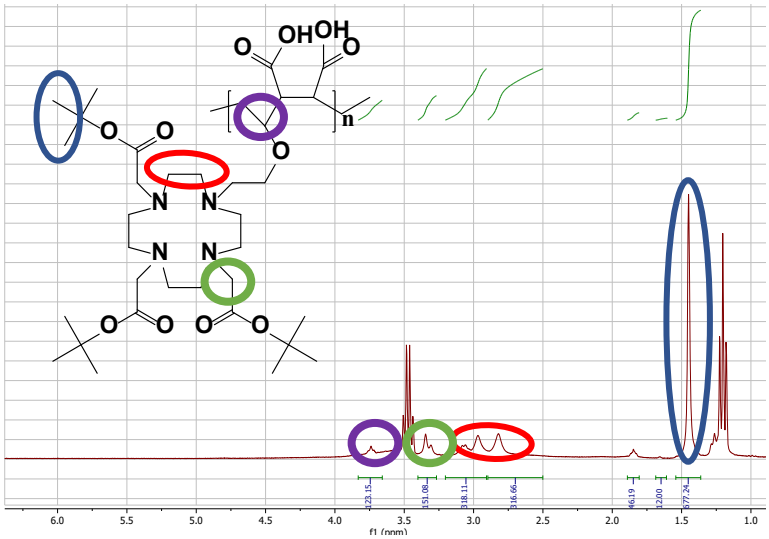

Figure 2.9) NMR 1,4,7,10-tetraazacyclododecane-1,4,7-tris(tert-butoxycarbonylmethyl) ethyl vinyl ether co maleic anhydride (CEVE-co-MA)

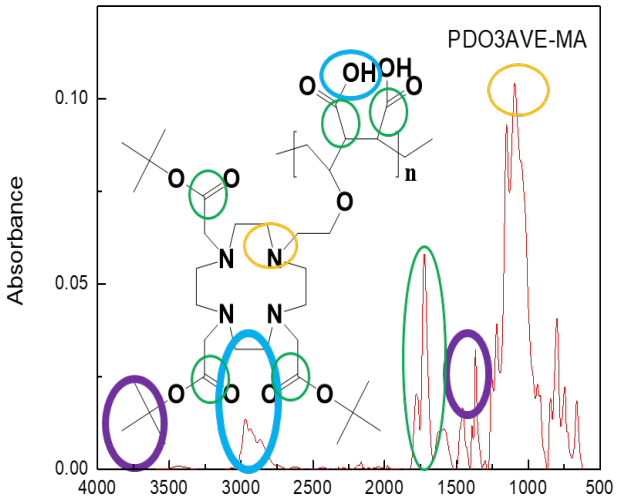

Figure 2.10) FTIR of 1,4,7,10-tetraazacyclododecane-1,4,7-tris(tert-butoxycarbonylmethyl) ethyl vinyl ether

2.5 Synthesis of modified Gd- 1,4,7,10-tetraazacyclododecane-1,4,7-tris (*acetic acid*) ethyl vinyl ether co maleic anhydride

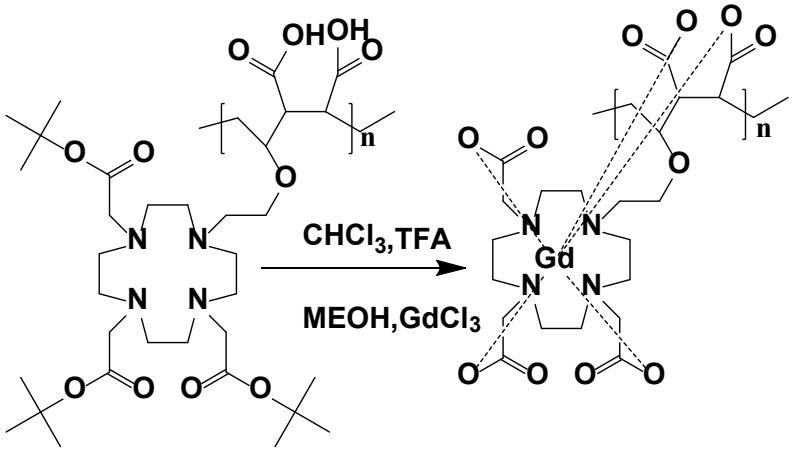

Figure 2.11) Scheme of Modified Gd- 1,4,7,10-tetraazacyclododecane-1,4,7-tris (acetic acid) ethyl vinyl ether co maleic anhydride

The next step in our synthesis is a deprotection of the t-butyl esters groups into carboxylic acids. Deprotection was done using trifluoracetic acid (TFA) in excess to cleave the t-butyl ester into in carboxylic acid, after which gadolinium (III) chloride was added to for chelation forming the corresponding structure. The product was then further put through dialysis for two days, followed by lyophilization. The concentration of gadolinium in the sample was then characterized using ICP-MS with the isotope of gadolinium that was selected was Gd 157 as that was the most abundant isotope that provided no interference. In order to make sure that we get the correct concentration, a sample of the known amount was dissolved in a known amount of water in which it was pipetted into different scintillation vials at different volumes. The solutions were then put into an oven

for 24 hours at 500 ℃ to decompose the organic polymer. After 24 hours, there was no observable matter in the glass scintillation vials. Then 15 ml of 2% w/v nitric was added to the vials, which was then placed into 15 ml centrifuge tubes. The samples were then taken to L.G. Rich Environmental Research Laboratory to have the samples analyzed through ICP-MS.

2.6 MRI contrast properties of modified Gd- 1,4,7,10-tetraazacyclododecane-1,4,7-tris (acetic acid) ethyl vinyl ether co maleic anhydride

The MRI analysis was done at the University of Alabama at Birmingham inside a 3 Tesla siemens MRI in which the department of neurology obtained the scan. The experimental setup consisted of a bucket filled with water with our sample holder that was then placed in a headspace coil, as shown in figure 2.12**.** In order to provide a better signal to noise ratio, the water in the bucket had 10 ml of ProHance to shorten the T_1 and T_2 of the background. The preparation of the samples was done by picking concentration of polymer was picked at certain concentrations as well as the calcium levels such that there were several chelate concentrations. These several concentrations were repeatedly made, only changing the calcium concentrations. Our initial studies involved calcium levels in the physiological range, such as 0 to 1.5 mM of calcium. While other studies show calcium levels at different ranges. Moreover, the [Ca]/[COOH] was also compared. Comparing the [Ca]/[COOH], in a way, gives some insight into how well this polymeric contrast agent interacts with calcium. The sequencing for T_1 and T_2 was chosen through

the University of Alabama, Birmingham. The T_1 sequences involved TRs at 4 seconds and predetermined IRs of 25, 50, 250, 500, 750, and 1200 milliseconds for the T_1 measurements. The corresponding T_2 sequence uses 32 TEs and a TR of 4 seconds to help generate the T_2 images. The T_1 and T_2 images were then used to create T_1 and T_2 maps using MATLAB software.

Figure 2.12) Image of experimental set up with the sample holder inside a head space coil a bucket filled with ProHance water surrounding the samples

Briefly, the T_1 and T_2 images are imported into MATLAB in which then each pixel on each image undergoes an exponential curve fit, which is then exported out of MATLAB into a

corresponding dicom image called either a T_1 or T_2 map. An example of mapping is shown in figures 2.13 and 2.14, showing T_1 and T_2 mapping, respectively. Furthermore, in the image of the T_1 mapping shows how the relaxation times of T_1 were obtained through the exported dicom image. The software, RadiAnt, translates the pixel intensity of each voxel and gives out a corresponding average T_1 time with max, min, and standard deviation over the area analyzed.

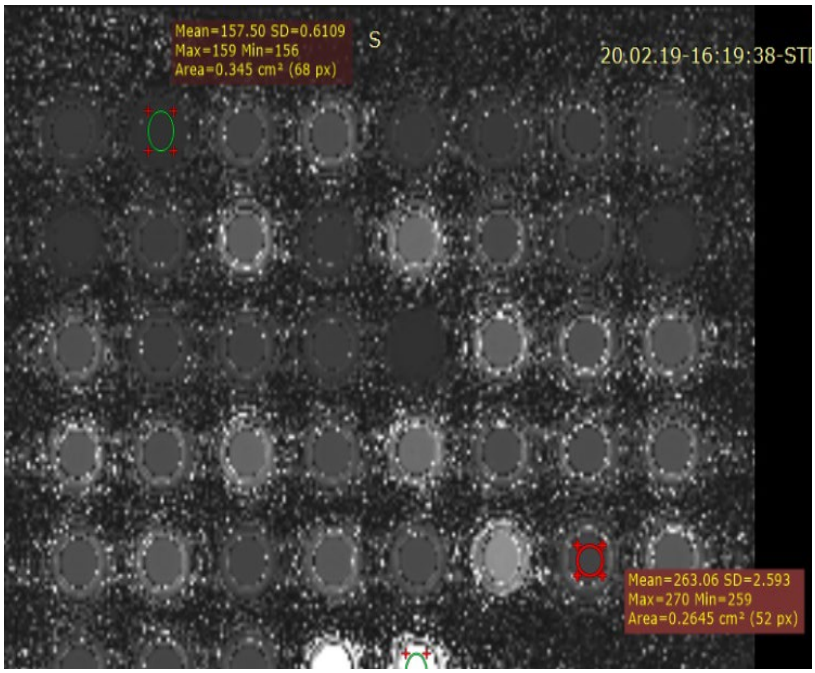

Figure 2.13) Example of T_1 mapping with how to get the corresponding T_1 vales of each sample from the using RadiAnt as the software

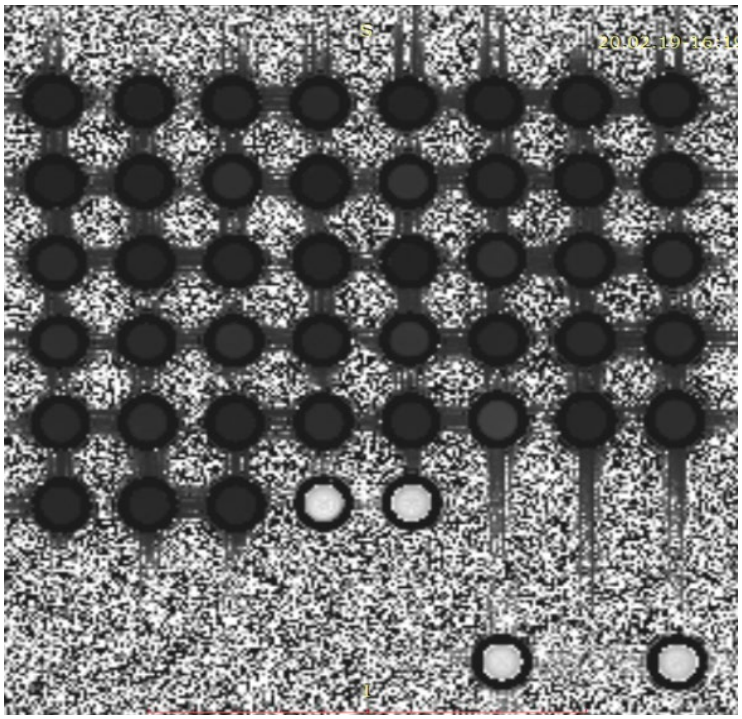

Figure 2.14) Example of T_2 mapping

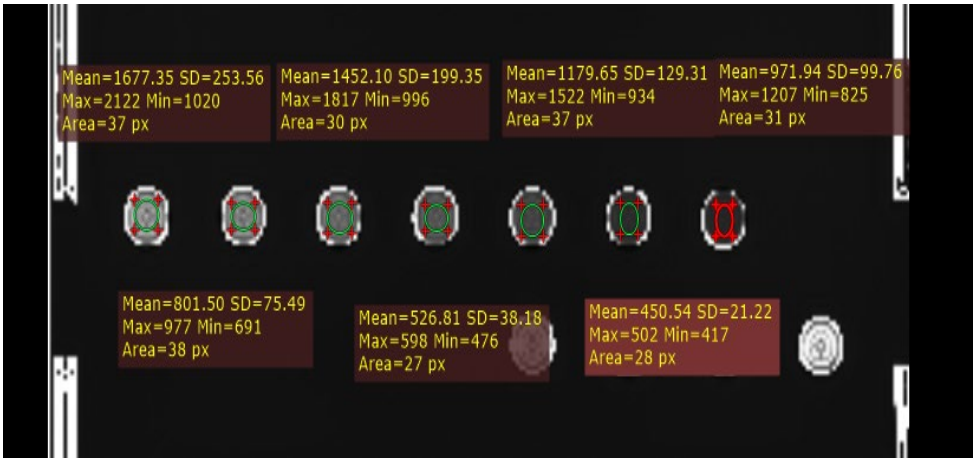

Figure 2.15) T_1 mapping of ProHance

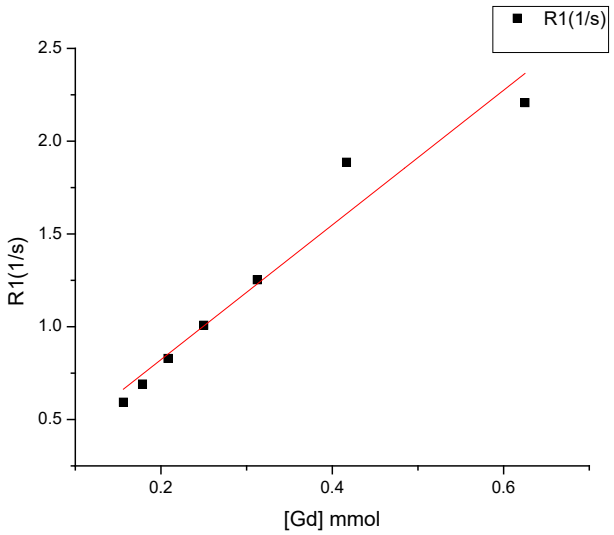

Figure 2.16) T1 mapping of relxativity as a function of Gd concentration of ProHance with an R- squared value of 0.94

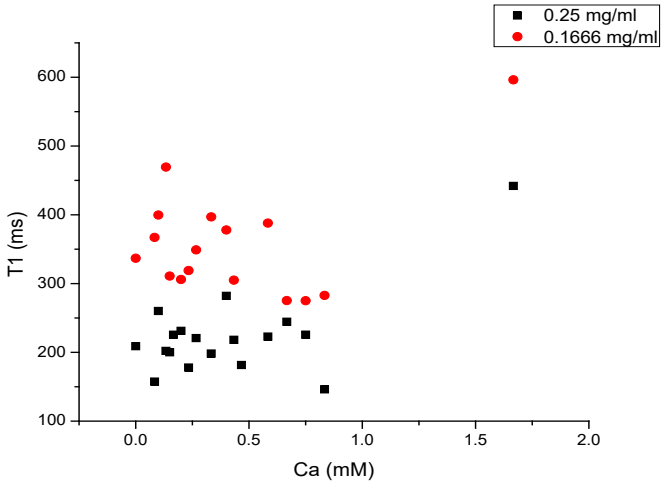

Figure 2.17) Graph of T_1 vs calcium concentration for 0.25 mg/ml and 0.01666 mg/ml

Each T1 time was then recorded into an excel spreadsheet keeping note of the known

polymer and calcium concentrations in each endorphin tube. However, before we conducted the experiments one of the first experiments that were done was the use of a known contrast agent for us to make comparisons and this is shown in figure 2.12, along with figure 2.16 which indicates the relaxivity generated from figure 2.15

The selected contrast agent used was ProHance for comparison. The reason for this is because of its structural similarity to the chelate component of our polymeric contrast agent. The results indicate an R-squared value of 0.9485 with a linear slope of 2.3643 L/mmol S in deionized water. This compares similarly to the reported values of ProHance of about 2.6 L/mmol S., Indicating that the MRI system acceptable to use for quantitative measurements. The same was also done with Gadvist (gadobutrol) which is another FDA approved contrast agent with known relaxation times and measurements The results were then plotted in several ways to help better understand the data. First, the T_1 times were plotted as a function of calcium. Several plots are shown in graphs 2.14 that showed the attempt to demonstrate the effect that calcium had on the system. Furthermore, an analysis was also compared with just DI water and samples of ProHance to indicate if the MRI scanner was working as intended.

The sample of polymer concentration with corresponding values of 0.25 and 0.1666 mg/ml shows relatively flat dependence on calcium until the concentration approaches one mM of calcium concentration. Then afterward, it is followed by a gradual increase after calcium levels reach high elevation. What is also observed what appeared to be is that as the concentration of polymer drops, the dip around 1mM becomes less and less

pronounced. However, there is still a gap in the calcium levels that we are examining, so further analysis is needed to exhibit this behavior. For this, a new series ran to help fill the gap between the 0.6 mM and 0.8 mM. Unfortunately shows no indication of calcium response. We then looked at the results more closely we thus, we did construct plots of moles of Ca and moles of COOH as shown in graphs 2.18 for the 0.25 mg/ml series. In a theoretical scenario, it would take one free calcium ion per 2 carboxylic acid giving a max ratio of 0.5 [Ca]/[COOH] in an ideal case. When looking back previous literature on calcium-sensing ions such as Angelovski et al., work his macromolecule seemed to demonstrate a similar effect with the shortest T_1 time being around 2 [Ca]/[polymer concentration] or about 1 [Ca]/[COOH] (21). Looking back at other literature, examples such as the publication of the work of a Barandov et al. showed his molecules have a [Ca]/[COOH] of around 1 to 1.5, both demonstrating where the onset where his relaxivity curve starts to behave asymptotically. Leading to suggesting

evidence that a [Ca]/[COOH] ratio of around 1 to 1.6 indicate that once the

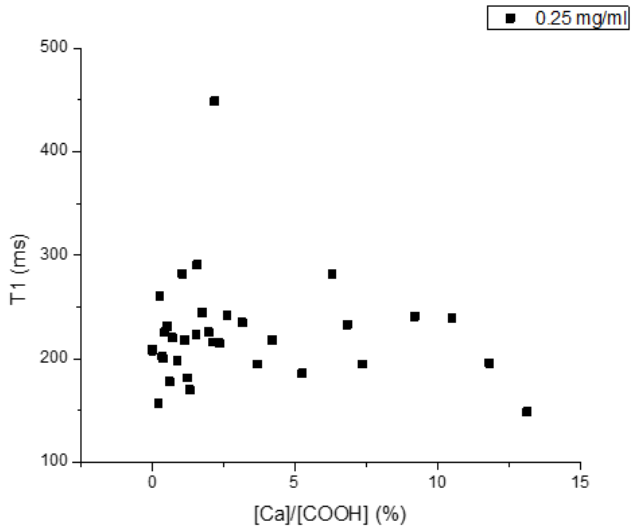

Figure 2.18) Graph of T_1 vs [Ca]/[COOH] for 0.25 mg/ml chelate

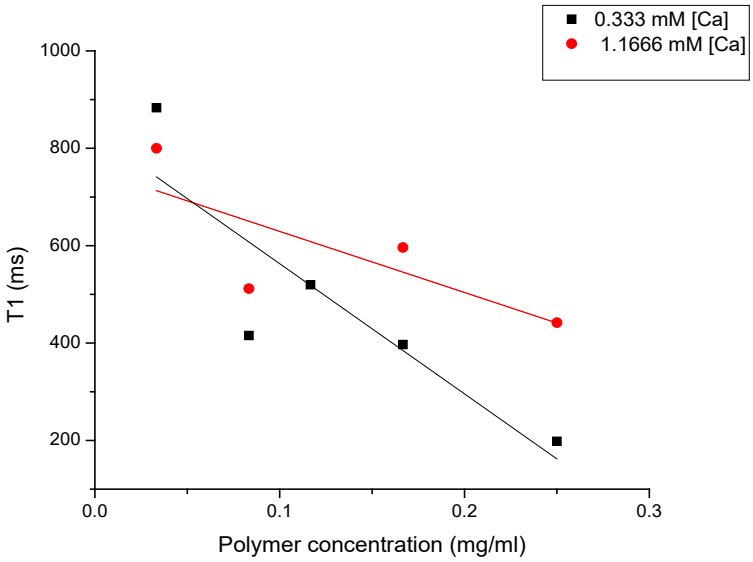

Figure 2.19) Graph of T_1 vs constant calcium levels of 0.3333 and 1.6666 calcium concentration at 0 mM and 0.0833 mM of free calcium with R-squared values of 0.59 and 0.77 respectively

Macromolecules are saturated with calcium. The T_1 values and relaxivity values do not change very much. It is shown that we didn't exhibit the same dependency, as shown in graph 2.18**.** Instead, a relativity flat line between T_1 and Ca/COOH indicating that the is no observable behavior between T_1 and the ratio between Ca/COOH. Potential reasons for this could be simply of structural repeat unit is simply not robust enough. To further elaborate previous literature uses BAPTA modified macromolecules, which provide two advantages. The first is that this molecule consists of four carboxylic acid groups readily available to bind the calcium as opposed to two.

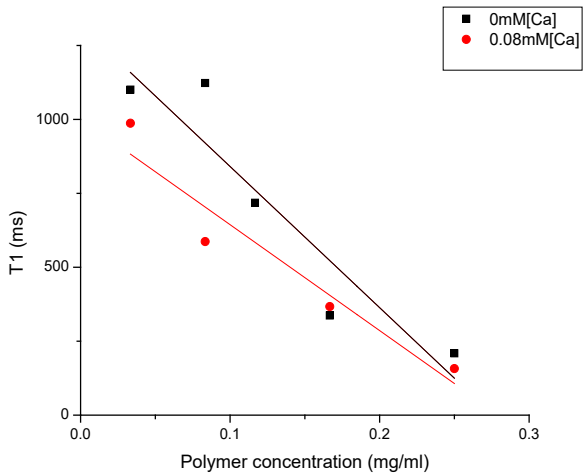

Figure 2.20) Graph of T_1 vs Constant calcium levels of 0 and 0.08333 calcium concentration at 0 mM and 0.0833 mM

The next is that the backbone on our polymer contains a rather ridged carboxylic acid group. This means that the spatial conformation is limited to that of BAPTA and thus can lower binding affinity to free calcium ions. Other possibilities may suggest that since the

product was imaged in DI water, that it may not have a strong enough binding affinity to the calcium ions due to it being a close to neutral pH. This idea was, however, partially investigated. The pH of the solution was measured by both pH paper and pH probe, with only slight differences examined between the two. Overall, the pH of the solution was found to be about 7.3, which is a slightly basic environment. However, the samples were prepared at different concentrations at constant calcium levels. This is shown in figures 2.20 at was shown here is the comparison of the R squared values and the linear equations. What is shown is that at low calcium levels, the equation that is referenced in chapter one, equation 1, proves to be true. However, if the calcium levels increase, the linearity in the curves starts to shift, showing no significant relationship between polymer concentration and the relaxation time. The results demonstrate that it shows not only T_1 change but that linear relationship between the concentration of gadolinium and the observed relaxation rates also change with varying levels of calcium concentration. In exaggeration, the linear constant [R_1] shown in equation 1 to give an idea of how effective other contrast are no longer become a valid form of measurement for this contrast agent—indicating a possible way that calcium levels influence the system our polymer water interaction. We also wanted to examine how our polymer played a role in T_2. As shown in figures 2.21 what was discovered was that the T_2 curves showed similar results as T_1 and that the only significant difference is that the relaxation times for T_1 are great than the relaxation times for T_2 meaning that T_2 is always shorter than T_1 and this is to be expected in all cases for MRI measurements. The effect of T_2 shorting can be attributed

to the fact that these are macromolecules that pose a heavy influence on T_2. The mechanism is the slowing water protons rotation and diffusion processes.

Moreover, this could also exemplify the effect of the hydrogen bonding between our polymer backbone and the free water protons, and this will also start to reduce T_2 times. Only three considerations attribute to this effect. The first is the size of the particle. The second is the concentration, and lastly is the types of functional groups the polymer is composed of (32-34). However, for graph 2.23, there is not an obvious correlation between [Ca]/[COOH]. The reason could be due to the already short T_2 times that are examined—thus making the results having a baseline effect.

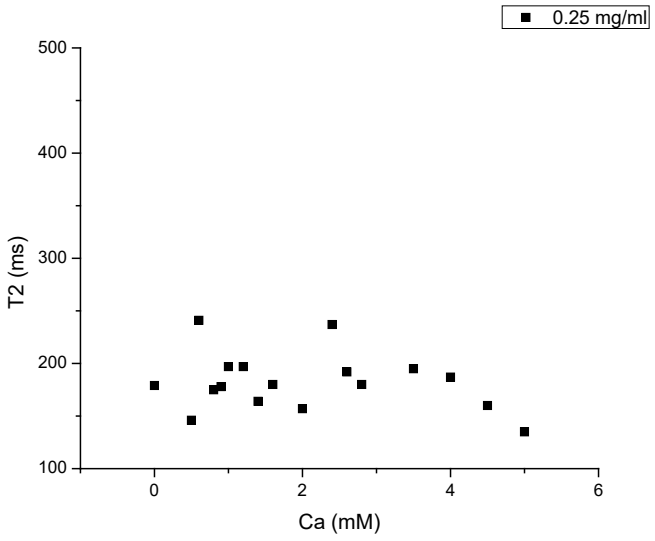

Figure 2.21) Graph of T_2 vs Calcium Concentration for 0.25 mg/ml

2.7 Potential error in measurements

As stated in this work, the T_1 and T_2 mappings were done through a MATLAB code. However, original mapping was done through Siemens using their software, and what was discovered was that each sample varied in T_1 mappings by about 300ms. How the mapping was generated can attribute to this effect. A stated before IR times of 25, 50, 75, 100, 250, 500, 750, 1000, and 1200 were conducted. However, the siemens software only takes two IR times for analysis, while our MATLAB code makes all the IR times to generate the mappings. We believe that since our map was constructed with more data points that it is more accurate to the actual T_1 times as opposed to the siemens software. In terms of the T_2 analysis, there was a little discrepancy with the mappings. This is likely because, just like the Siemens software, our MATLAB code takes into account all the echo times (TE), and thus the measurement is similar. Further investigation should be done to get the measurements more in accordance since this is for quantitative use. Nevertheless, the trending from the measured T_1 and T_2 are similar regardless of software and that these only affect just the measured T_1 and T_2 relaxation times. Thus the trend from reach graph represented in the chapter is still valid.

2.8 Dynamic light scattering measurement

Dynamic Light scattering measurements (DLS) were done on the samples varying in pH as well as calcium concentration to attempt to understand why no significant calcium response was observed. In previous literature Thomas Swift, Linda Swanson, a Mark Geoghegan, and Stephen Rimmer examined global to coil transitions based on the varying

effects of pH for polyacrylic acid(35). As shown in there study, the pH affects the molecular weight showing that a pH of a more acidic solution provided a more globular shape. In contrast, a higher pH produced a more linear chain conformation in their experiment. Furthermore, other studies also show that if pH changes with copolymers of N-isopropyl acrylamide, they also examine this coil to globular transition as pH was changed (36). Due to the nature of theses polymer to be able to carry charges species on their backbone. What was hypothesized is that our polymer showed aggregation. This could explain why there was shown no calcium response in the polymer. The exaggeration would not allow into the polymer backbone and thus limiting the calcium sensitivity of the polymer. For this, a light scattering experiment was conducted with the results located in appendix A.1 As shown in the results, the pH of the first polymer solution in DI showed a size of about 700 nm in diameter. Afterward, calcium chloride was added to adjust the calcium level in the sample to 0.5 mM, then 1mM, as shown the overall change in diameter, did not change very much, which suggests that calcium has little influence on the system. Then the pH was adjusted on the polymer system to see how that influenced the size measured by DLS. For this, the pH was adjusted to 1 and 14. What was shown in both ways that the DLS measurements showed a slight increase in particle size to 1200 nm in size. In all experiments, the measurements of the particle sizes proved to be quite large, perhaps indicating that there is aggregation forming from our particles, and that is why there is no calcium response as opposed to a globular conformation. Our size Also, the system may show a slight sensitivity to pH. Previous literature indicates that

DLS measurements for polyethylene glycol in the work of Nelson and Cosgrove demonstrated that PEG, a high molecular weight (1,000,000 g/mol), had a 10 nm hydrodynamic diameter(37). Furthermore, pertaining to the work of Melinda, Bodar, Hartmann, and Borbely, it was demonstrated that polyacrylic nanoparticles crossed linked gave a hydrodynamic diameter of 120nm (38). Similar work in Zhenyuan Qu, Fenglin Hu, Kaimin Chen, Zongqiang Duan, Hongchen Gu, Hong Xu conducted DLS measurements on their colloidal particles with a max measurement of 500nm (39). Since the DLS measurements around are samples, indicate at size on the order of 0.7 to 1.2 microns leads evidence to suggest that the polymer contrast agent is forming aggregation and thus is starting to represent measurements like a colloidal suspension as opposed to a dilute polymer solution. Working through calculations for the dynamic size of the polymer using the equation $R_h = K M_w^{(a)}$ (3) where R_h is the hydrodynamic radius, K is a proportional constant, M_w is the molecular weight, and a can range from 0.5 to 3/5 depending on if the solvent is a good solvent or not. In our case, we will use an estimation based on the parameters of PEG, K = 0.145, and a = 0.571(40). In our case of this polymer, our hydrodynamic diameter is calculated to be 57.9 nm in hydrodynamic diameter. Moreover, an alternative way to calculate hydrodynamic diameter is us using the following equation ($R_h = KT/(3 \pi (\mu)D)$) (4) Where K is the Boltzmann constant, T is the absolute temperature, μ is the viscosity and D is the translation diffusion coefficient. In our case, we will use Abohachem Laguecir Serge Ulrich, Jerome Labille, Nicolas Fatin-Rouge, Serge Stoll, Jacques Buffle with polyacrylic acid to approximate the hydrodynamic diameter of our

polymer using a diffusion coefficient of $0.4(cm^2/s*1x10^6)$(41). After numerical calculation, the resulting hydrodynamic diameter is 1.2 nm in size. In both theoretical calculations, our measurement is much larger. Therefore, this provides some evidence to support that we do have aggregation.

2.9 Conclusions

Inconclusion, a successfully synthesized polymeric contrast agent, was made and characterized through FTIR and NMR along with each step that was characterized through NMR and FTIR. The magnetic resonance imaging measurements show that there is no noticeable change in T_1 times vs. calcium. Therefore, there is no noticeable change in R1 rates versus calcium since in two a reciprocal of each other. However, the linear linearity of the T_1 vs. chelate concentration does change as calcium levels are changed, giving this some potential to be still used.

Conclusively, results seem to indicate no changes in response to calcium other than the shift of linearity. The progress made here gives a good insight into why chapter three is so important for the future of ion sensing contrast agents. Further investigation is still needed to understand its lack of calcium responsivity. In chapter 3, the approaches made will help rectify some of the potential issues in chapter 2 as it takes more of a similar approach from literature.

CHAPTER 3

Potential improvement of first design using controlled polymerization

3.1 Introduction

The results from chapter 2 indicate some potential for an ion sensing polymeric contrast agent. However, this initial design is not without its flaws. One of the first issues of the polymeric contrast shown in chapter 2 in the control of molecular weight since it is a free radical polymerization its disparities can vary and provide a wide range of molecular weights. This, in turn, could affect some of the MRI contrast properties that were also shown in chapter 2. Furthermore, common calcium chelating agents, as stated in chapter 1, such as EDTA or BAPTA, have four carboxylic acid groups as opposed to our two carboxylic acids for the structure in chapter 2. Lastly, our polymer structure in chapter 2 may not be selective towards just calcium ions but may be susceptible to other divalent ions such as magnesium. This chapter aims to examine an alternative polymeric contrast agent that aims to address some of the issues with the structure in chapter 2. For this approach, we wanted a controlled polymerization for finely controllable molecular weight as well as the use of a calcium dye (BAPTA), which has been proven to a great calcium chelator over other competing ions. For this, we have proposed two synthetic pathways that have the potential to lead to the final product, as shown in Figure 3.1. In each pathway involved is a controlled ionic polymerization. The first path was to construct a polymer then modify the polymer with two potential function groups for this reaction strategies were taken out of the work of Kim, Kweon, and Noh using $BF_3(OEt)_2$ as the

initiator(42). The next one involves monomer synthesis then polymerizing at the end to produce our statistical copolymer. For this, we try modifying our epoxide ring with a ring-opening using either a primary or secondary amine. Then later, a ring-closing reaction is done to reform the epoxide ring. The ring closed product could then be polymerized. This strategy constructed created from examples listed by Saddique *et al.* 2016 (43).

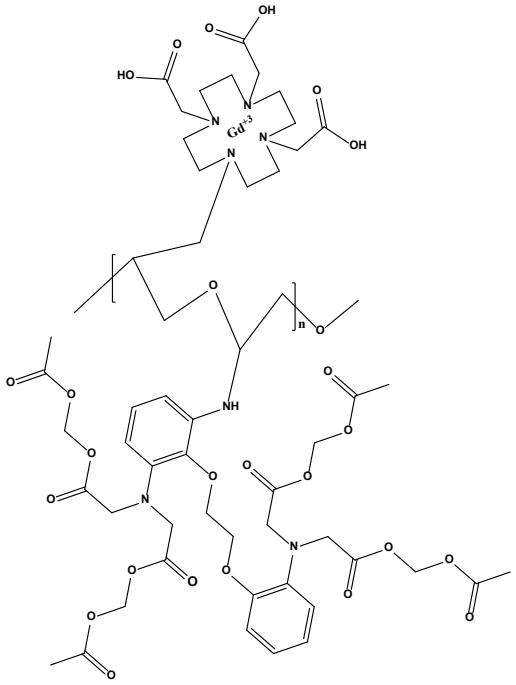

Figure 3.1) Image of repeat unit structure of new repeat unit using ether backbone that is both modified with BAPTA-AM and PDO3A.

3.2 Nitration and reduction of BAPTA

The nitration of BAPTA was done by dissolving BAPTA in dimethyl sulfoxide then added 1.5 equivalent of sulfuric acid with 1.5 equivalents of nitric acid over dropwise into the flask contain DMSO-BAPTA solution at room temperature. Then the reaction could stir overnight. The reaction scheme can be shown in figure 3.2. Afterward, the product in DMSO underwent lyophilization to remove DMSO, water, and acid from the solution. The carbon 13 NMR was done for structural identification. Then the nitrated BAPTA was dissolved in DMSO with the addition of Pd/C, which was then allowed to stir overnight in the open air. This process allowed for the reduction of the nitro group into a primary amine. The full reaction is as follows, the nitrated BAPTA (n-BAPTA) was added to a 50 ml flask was added to in with ethanol at room temperature. Then the Pd/C catalyst was added to the solution in 50 mg/mmol of substrate. The hydrogen gas was produced by dripping methanol into a suspension of sodium hydride and hexane and routed such that the hydrogen gas was able to bubble through the reaction solution. This reaction proceeded for 40 minutes before the reaction was stopped. The full reaction setup can be seen in the appendix A.2.

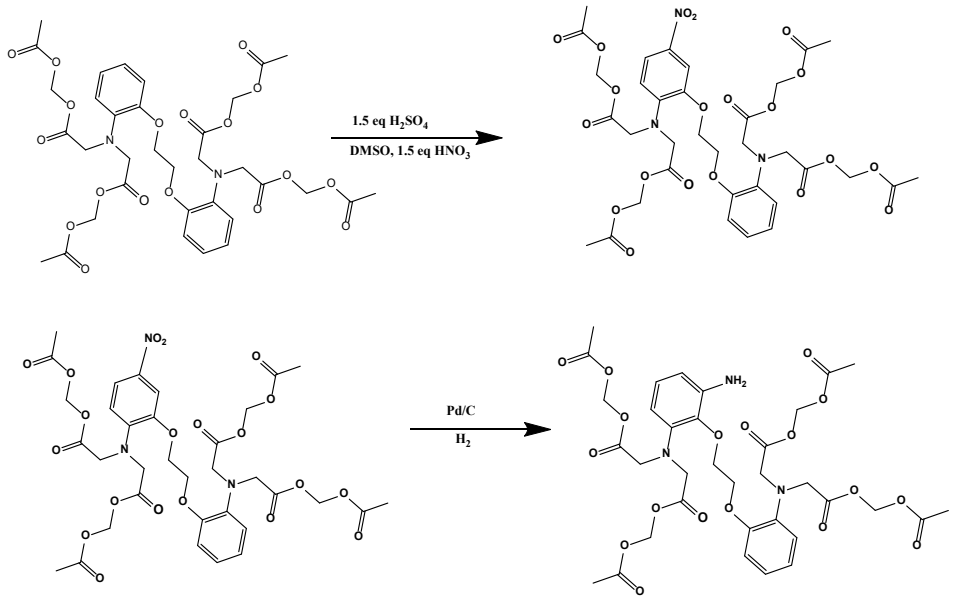

Figure 3.2) Nitration of BAPTA then reduction using palladium on carbon to reduce nitro group into primary amine

3.3 Pathway number 1

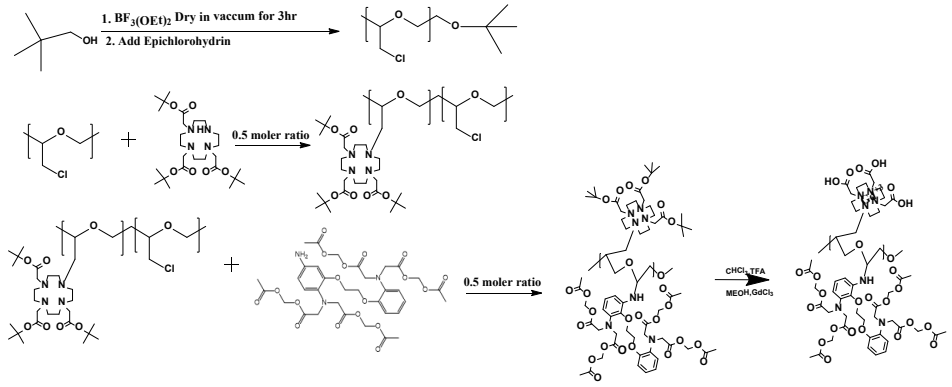

Figure 3.3) Theoretical reaction scheme starting with polymer synthesis

In this pathway, we first take t-butyl alcohol and react it with $BF_3(OEt)_2$ with the addition of epichlorohydrin. The process is named a cationic polymerization reaction. The monomer and initiator ratio was picked, such that the target molecular weight is 10,000 g/mol. This was done by using the following procedure described in Kim, Kweon, and Noh's work(42). Briefly, $BF_3(OEt)_2$ was added to a 250 ml flask, which was then put under vacuum. Then dry dichloromethane was then added to the flask. Afterward, the addition of epichlorohydrin was added dropwise to the flask at room temperature. The reaction was then allowed to react overnight, then was reduced under pressure and then precipitated in hexane. The product was then collected and analyzed. Using NMR, FTIR, and GPC. The NMR showed in figure 3.4 indicates the presence of an ether backbone and the presence of the end group. The FTIR shown in figure 3.5 had shown the indicated functional groups, while the GPC shown in figure 3.6 showed the molecular weight was low compared to polystyrene samples. The peak area of the lowest standard using the RI dictator is 436 in figure 3.6, with our sample peak being 11.1, as shown in figure 3.7. This indicates that we have the formation of oligomers, which is evidence to suggest that the reaction was terminating early the potential issues for this could be the water in the flask at the time of the reaction or potential branching repeat units causing the reaction to terminate early. Further investigation is required; however, it does show early signs of success.

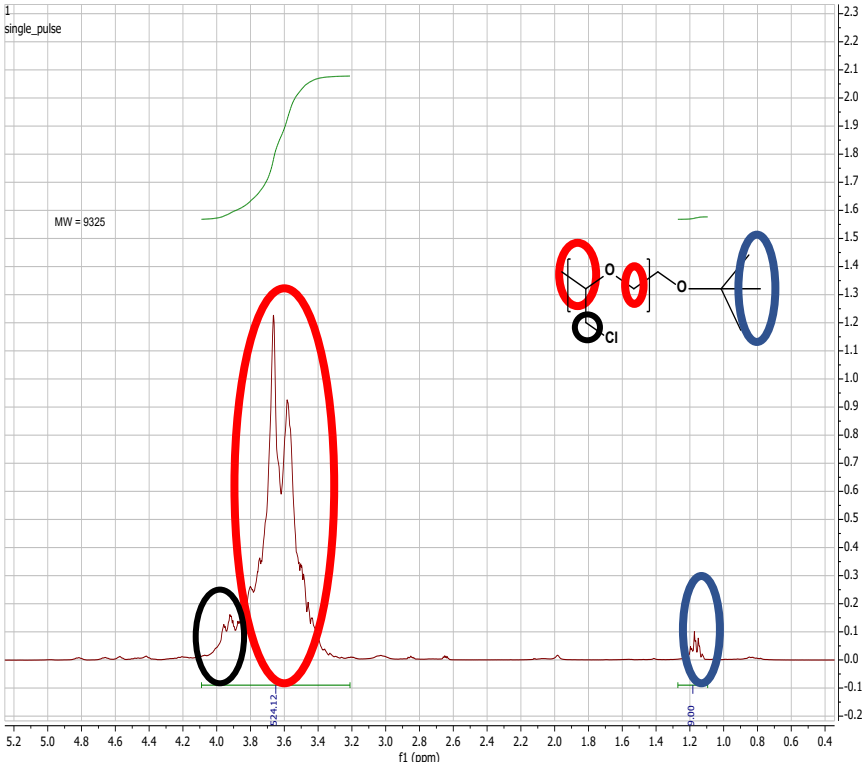

Figure 3.4) Proton NMR of PECH polymer

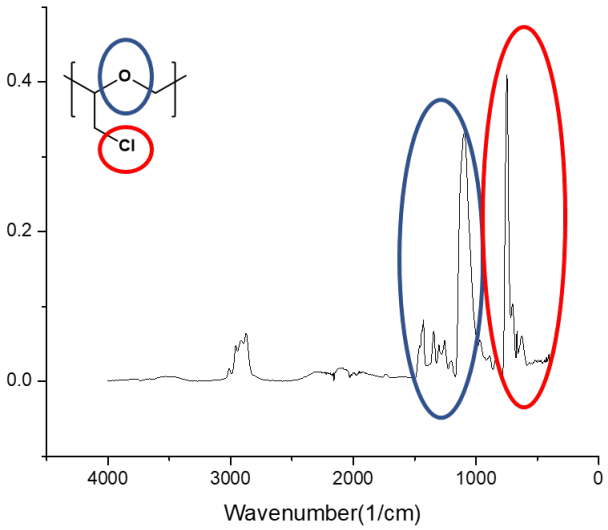

Figure 3.5) FTIR of PECH showing formation of ether backbone and halogen

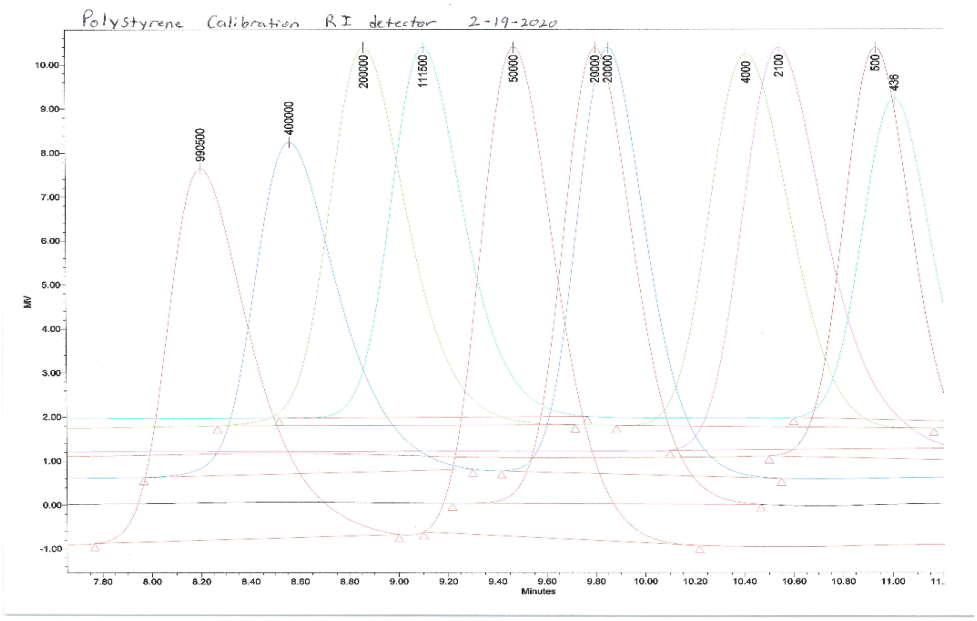

Figure 3.6) Polystyrene GPC standards going from 500 to 99,000 g/mol

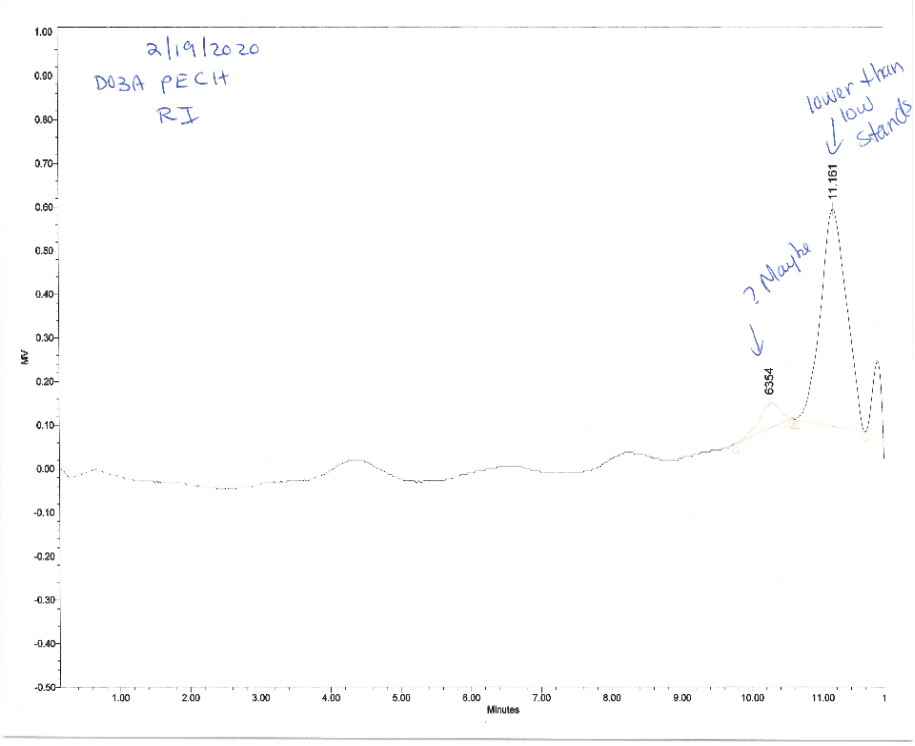

Figure 3.7) GPC elution of the sample showing 11.151 as g/mol as molecular weight by polystyrene standards

The next step of the process is to react the PDO3A as synthesized in chapter 2 with the chlorine in 0.5 molar equivalent using some base to help the nucleophilic attack then react the primary amine on the BAPTA with the other 0.5 molar chlorine of the epichlorohydrin. Then following similar procedures in chapter 2 for deprotection, react the polymer with trifluoracetic acid in 3 molar equivalent for 24 hours followed by evaporation of the acid in which an NMR and FTIR should then be taken. Finally, the last step should be to chelate with gadolinium (III) chloride hexahydrate for at least 24 hours, followed by a purification process and characterization of ICP-MS.

3.4 Pathway number 2

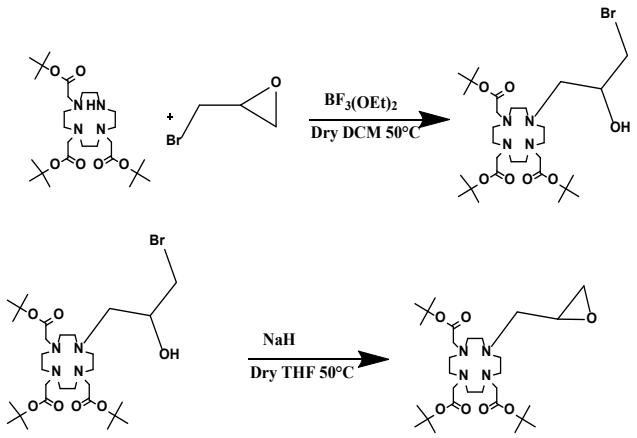

Figure 3.8) Second proposed pathway for synthesis 2.0

The second pathway involves synthesizing the monomer first before the polymerization the advantages of this is that the reaction can either be cationic or anionic polymerization. For this, nitration and reduction of the BAPTA is needed to be as shown in 3.1. Afterward,

the addition of $BF_3(OEt)_2$ was added in 1:1:1 molar equivalent of the POD3A and the Epichlorohydrin under an inert atmosphere at 55 °C**.** The reaction was done in the following steps. First, the flask was flamed dried and purged with nitrogen, then $BF_3(OEt)_2$ and Epibromohydrin was added to the flask with 10 ml of dichloromethane and was allowed to stir for 20 minutes at 55 °C. After this, a solution of PDO3A in 10 ml of dichloromethane was added dropwise into the flask and allowed to stir overnight. This reaction will force a ring-opening reaction, thus successfully modifying our PDO3A on to our substrate. Afterward, the reaction was then reduced under pressure and precipitated in hexane. As shown in the FTIR after purification, the presence of the carbonyl that is only presence on the PDO3A is still there as well as the presence of a hydroxyl group. This evidence suggests that there was a successful ring-opening reaction and that the EPI bromohydrin was successfully modified with the PDO3A chelating species. Followed after the FTIR and NMR analysis was conducted, as shown in figure 3.9, the presence of the t-butyl esters protecting group, which also indicates that there was a successful ring-opening reaction and that the secondary amine on the PDO3A was successfully converted into a tertiary amine.

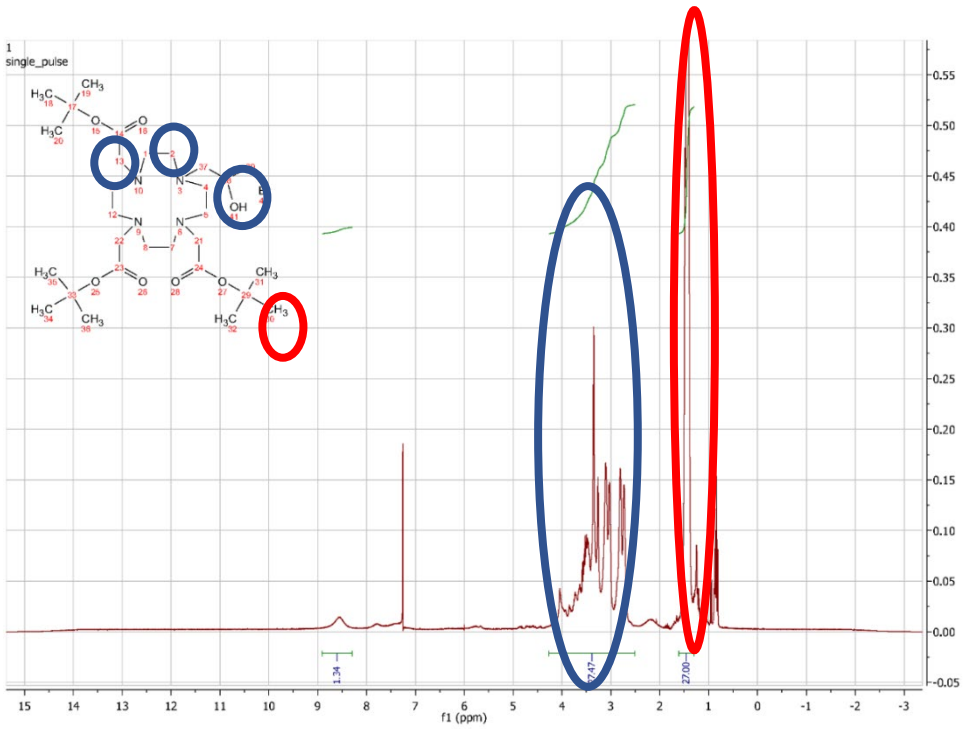

Figure 3.9) NMR of Ring opened product of PDO3A with Epibromohydrin

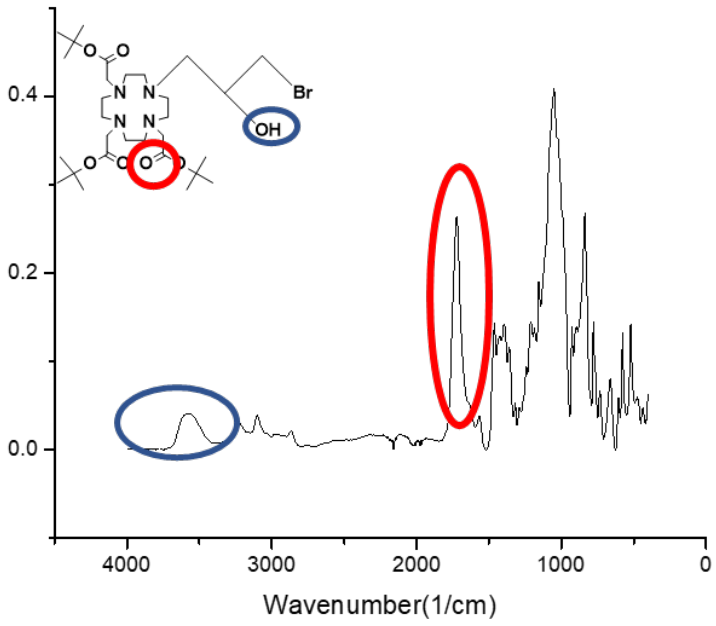

Figure 3.10) FTIR of ring opened product of PDO3A with Epibromohydrin.

In this case, both the NMR and the FTIR are in agreement with the ring-opening reaction.

Afterward, the product was then treated with sodium hydride in 1.5 molar excess. The sodium hydride will deprotonate the oxygen and force the intramolecular ring-closing reaction. The reaction was done at 50°C overnight. In which the product was then reduced under pressure and precipitated in hexane. Then an FTIR was taken of the product as shown in figure 3.9 there an OH stretch peak at 3500 wave number after the ring-opening reaction and then after the reaction with sodium hydride as shown in figure 3.9 there is no longer any OH stretch at 3500 wave number indicating that the was removal of the hydroxyl group showing that the reaction was then ring closed.

A similar reaction is done with the primary amine on the BAPTA and $BF_3(OEt)_2$ with the epichlorohydrin. Afterward, the two monomers would then be copolymerized using an anionic initiator of potassium bis trimethylsilyl amide would be used. It was chosen because of its ability to easily be disquisition NMR as well as its ability to be reduced to a primary amine after treatment with an acid such as trifluoroacetic acid. This provides it with more functionality for potential later uses. The potential reaction scheme is shown in figure 3.12

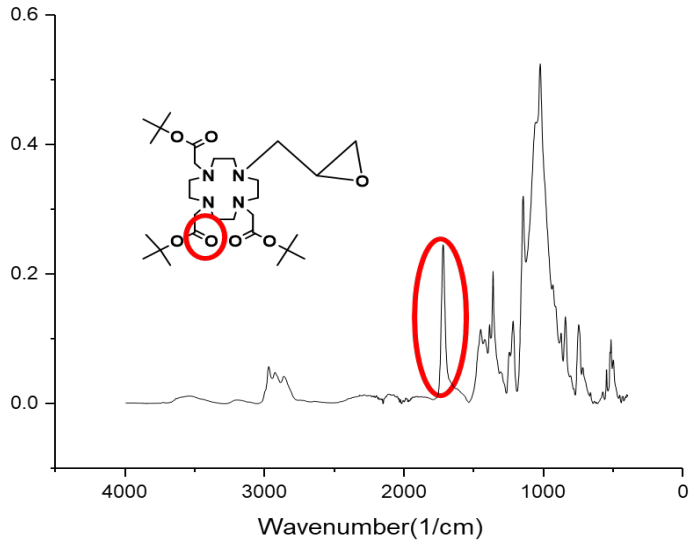

FTIR of ring closing product of PDO3A with

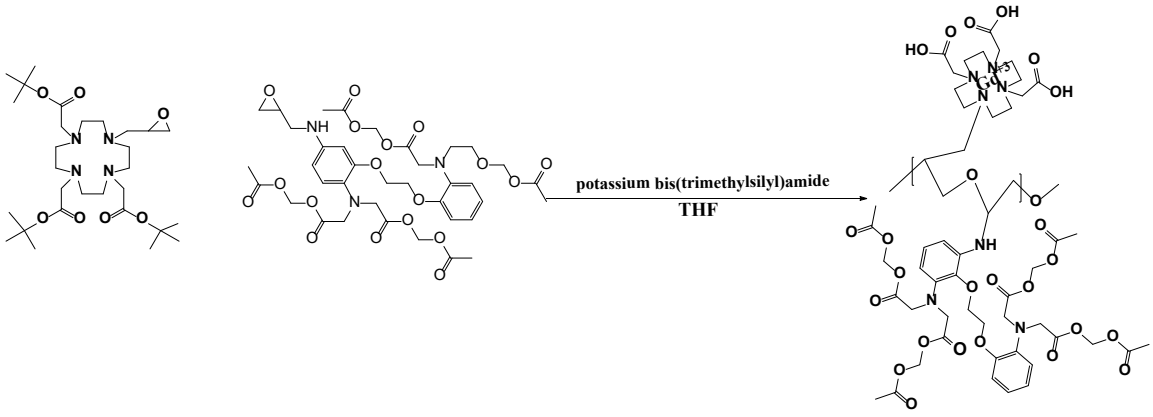

Figure 3.12) Proposed anionic reaction for pathway two done with the two-monomer synthesis

3.4 Discussion and future work

The goal of chapter 3 was to provide two particular synthetic pathways for potential improvement from the theory derived in chapter 2. There are still some issues with each synthetic route to work out its optimal workup and reaction conditions. The most promising route so far has been the synthesis of the monomer before polymerization. This is likely since this reaction is not as water sensitive as the cationic polymerization. The FTIR before and after the ring-opening and ring-closing does show changes in the FTIR around 3500 wavenumbers showing the loss of alcohol peak. Showing evidence that the ring-closing reaction was successful. This potentially shows epoxide ring formation after reaction with sodium hydride. Also, the same reaction ring opening followed by a ring-closing reaction for after the nitration of the BAPTA-AM calcium chelator accurately synthesized and characterized with FTIR and NMR.

Moreover, for future work, the polymerization of the two monomers should also be done with reaction conditions yet to be determined likely plans for to perform the reaction at -20 °C followed by a workup and then an NMR and FTIR of the final product. As well the deprotection of the t-butyl groups on the polymer backbone and chelation with gadolinium (III) chloride hexahydrate further needs to be done, as well as purification and characterization of how much gadolinium should be analyzed by ICP-MS. Finally, an analysis of its MRI properties needs to be conducted. The study should be like how the polymeric contrast agent in chapter 2 should be done.

CHAPTER 4
Conclusion and future work

4.1 Conclusion

All synthetic work has been successful and characterized by FTIR and NMR spectroscopy. However, the application for the designed structure in chapter 2 did not work as intended. This is still a step in understanding how ion sensing chelates. From the data, it was concluded that a more robust polymeric contrast agent is needed to probe the free calcium ions. Which still leads to needing development in chapter 3. The new and proposed polymeric contrast agent is more in line with how current literature approaches this problem.

The fundamental difference is that in chapter 2 the polymer synthesized consists of 2 carboxylic acids groups per repeat unit and is a quite rigid structure and the polymer designed mentioned in chapter three shows great promise as it also addresses these issues as well in the sense that it builds off already established calcium-sensing chelates more specifically BAPTA-AM. As mentioned, the cationic reaction in chapter 3 caused early termination likely due to the presence in the water. The ring-opening approach, then the ring-closing approach, provides a better synthetic route. This is because purification of the monomers can be conducted after the reaction then the polymerization can be done afterward. This would seem to provide better control over the synthesis and properties.

In conclusion, the polymeric structure in the chapter was successfully synthesized and characterized as well as the MRI properties examined as well as its effects of calcium on the polymeric structure. The ring-opening and ring-closing rection in chapter 3 was successfully carried out and characterized through FTIR and NMR.

4.2 Future work

In chapter 2 of this work, more information needs to be gathered on the non-chelating water-soluble polymer in order to further help establish the meaning of the DLS results. Such as synthesizing and producing polyacrylic acid or polymethacrylic acid and copolymerization of polyacrylic acid with maleic anhydride or copolymerizing polymethacrylic acid with maleic anhydride. Also, a more in-depth scattering study could be done such as small-angle x-ray scattering or static light scattering

Work that currently needs to be done is the predominantly from chapter 3. Such polymerization of the ring closed EPI-PDO3A hydrin, as mentioned in and the EPIBAPTA-hydrin, as mentioned in 3.2. Future work also includes successful polymerization into a statistical copolymer afterward, the deprotection of the protecting groups of the needs to be done using trifluoracetic acid followed by a workup and characterization using FTIR and NMR. Afterward, a Chelation using gadolinium (III) chloride hexahydrate allowing at least 24 hours for reaction in methanol. Finally, the characterization of the amount of gadolinium can be done using ICP-MS after dialysis to remove any remaining ions. Afterward, samples should be made in the physiological range of calcium between 0 and

1.5 mM with polymeric contrast ranges based on the results of the ICP-MS. Then finally, the same analysis done for chapter 2 can be done for chapter 3. Moreover, depending on the resulting test should be implemented to see how biocompatible the material is.

In terms of analysis development of MATLAB software was done to produce the T_1 and T_2 mappings of the samples. Still, when compared to the MRI software for mapping, it results varied in measurements meaning that there is an error in the measurement, and this needs to be further studied to reconcile the difference, and perhaps a better approach for how the mapping is made using MATLAB should also be further investigated.

Furthermore, in addition to the use of chapter 3 the can further built on using other calcium chelators such as FURA-2 as another potential modifier to our functional polymeric chelator due to its high affinity and ability to fluoresce under UV light gives an idea for a new candidate that could be both MRI sensitive and multifunctional (44).

Moreover, what hasn't yet been answer adequately in the thesis is the effect of molecular weight on both relaxation and ion sensitivity. After the work proposed in chapter three is done, it is recommended that several molecular weights be produced followed by an MRI study and then compare the relaxation times the relxativity constant of each contrast agent to see if there is a difference.

Furthermore, the biocompatibility of either product of chapter 2 or chapter 3 has yet to be tested. Thus a series of tests need to be done to see how compatible they are with biological systems, as well as studying the diffusion rates of the polymer throughout the body.

References

1. Krishnamurthy RV. Hydrogen isotopes. In: Geochemistry. Dordrecht: Springer Netherlands; 1998. p. 326-330.

2. Berger A. Magnetic resonance imaging. *BMJ.* 2002 Jan 5; 324(7328): 35. PMCID: PMC1121941.

3. Bydder G, Young I. MR imaging: Clinical use of the inversion recovery sequence. 1985.

4. Na HB, Hyeon T. Nanostructured T1 MRI contrast agents. *Journal of Materials Chemistry.* 2009; 19(35): 6267-6273.

5. Xiao Y, Paudel R, Liu J, Ma C, Zhang Z, Zhou S. MRI contrast agents: Classification and application. *Int J Mol Med.* 2016; 38(5): 1319-1326.

6. Clough TJ, Jiang L, Wong K, Long NJ. Ligand design strategies to increase stability of gadolinium-based magnetic resonance imaging contrast agents. *Nature communications.* 2019; 10(1): 1-14.

7. De León-Rodríguez LM, Martins AF, Pinho MC, Rofsky NM, Sherry AD. Basic MR relaxation mechanisms and contrast agent design. *Journal of Magnetic Resonance Imaging.* 2015; 42(3): 545-565.

8. Rinck P, Muller R. Field strength and dose dependence of contrast enhancement by gadolinium-based MR contrast agents. *Eur Radiol.* 1999; 9(5): 998-1004.

9. Hagberg GE, Scheffler K. Effect of r1 and r2 relaxivity of gadoliniumâ€based contrast agents on the T1â€weighted MR signal at increasing magnetic field strengths. *Contrast media & molecular imaging.* 2013; 8(6): 456-465.

10. Elster AD. Field-strength dependence of gadolinium enhancement: Theory and implications. *Am J Neuroradiol.* 1994; 15(8): 1420-1423.

11. Nanda H. Getting to the HEART of the MATTER. *Qual Prog.* 2019; 52(4): 38-45.

12. Que EL, Chang CJ. Responsive magnetic resonance imaging contrast agents as chemical sensors for metals in biology and medicine. *Chem Soc Rev.* 2010; 39(1): 51-60.

13. Rohrer M, Bauer H, Mintorovitch J, Requardt M, Weinmann H. Comparison of magnetic properties of MRI contrast media solutions at different magnetic field strengths. *Invest Radiol.* 2005; 40(11): 715-724.

14. Prince C, Bruhns ME. Evaluation and treatment of mild traumatic brain injury: The role of neuropsychology. *Brain sciences.* 2017; 7(8): 105.

15. McCrory P, Meeuwisse W, Dvorak J, Aubry M, Bailes J, Broglio S, Cantu RC, Cassidy D, Echemendia RJ, Castellani RJ, Davis GA, Ellenbogen R, Emery C, Engebretsen L, Feddermann-Demont N, Giza CC, Guskiewicz KM, Herring S, Iverson GL, Johnston KM,

Kissick J, Kutcher J, Leddy JJ, Maddocks D, Makdissi M, Manley GT, McCrea M, Meehan WP, Nagahiro S, Patricios J, Putukian M, Schneider KJ, Sills A, Tator CH, Turner M, Vos PE. Consensus statement on concussion in sport-the 5th international conference on concussion in sport held in berlin, october 2016. *Br J Sports Med.* 2017 06/01; 51(11): 838.

16. Young W. Role of calcium in central nervous system injuries. *J Neurotrauma.* 1992 Mar; 9 Suppl 1: S9-25.

17. Meythaler JM, Peduzzi JD, Eleftheriou E, Novack TA. Current concepts: Diffuse axonal injury–associated traumatic brain injury. *Arch Phys Med Rehabil.* 2001; 82(10): 1461-1471.

18. Weber J. Altered calcium signaling following traumatic brain injury. *Frontiers in Pharmacology.* 2012; 3: 60.

19. Bouschet T, Henley JM. Calcium as an extracellular signalling molecule: Perspectives on the calcium sensing receptor in the brain. *Comptes rendus biologies.* 2005; 328(8): 691-700.

20. Grienberger C, Konnerth A. Imaging calcium in neurons. *Neuron.* 2012; 73(5): 862-885.

21. Hanaoka K, Kikuchi K, Urano Y, Narazaki M, Yokawa T, Sakamoto S, Yamaguchi K, Nagano T. Design and synthesis of a novel magnetic resonance imaging contrast agent for selective sensing of zinc ion. *Chem Biol.* 2002; 9(9): 1027-1032.

22. Atanasijevic T, Shusteff M, Fam P, Jasanoff A. Calcium-sensitive MRI contrast agents based on superparamagnetic iron oxide nanoparticles and calmodulin. *Proc Natl Acad Sci U S A.* 2006 Oct 3; 103(40): 14707-14712. PMCID: PMC1595416.

23. Barandov A, Bartelle BB, Williamson CG, Loucks ES, Lippard SJ, Jasanoff A. Sensing intracellular calcium ions using a manganese-based MRI contrast agent. *Nature communications.* 2019; 10(1): 1-9.

24. Angelovski G, Fouskova P, Mamedov I, Canals S, Toth E, Logothetis NK. Smart magnetic resonance imaging agents that sense extracellular calcium fluctuations. *ChemBioChem.* 2008; 9(11): 1729-1734.

25. Barandov A, Bartelle BB, Williamson CG, Loucks ES, Lippard SJ, Jasanoff A. Sensing intracellular calcium ions using a manganese-based MRI contrast agent. *Nature Communications.* 2019 02/22; 10(1): 897.

26. Dwyer F. Chelating agents and metal chelates. Elsevier; 2012.

27. Flora SJ, Pachauri V. Chelation in metal intoxication. *International journal of environmental research and public health.* 2010; 7(7): 2745-2788.

28. Bartolini M, Pekar J, Chettle D, McNeill F, Scott A, Sykes J, Prato F, Moran G. An investigation of the toxicity of gadolinium based MRI contrast agents using neutron activation analysis. *Magn Reson Imaging.* 2003; 21(5): 541-544.

29. Harrison SM, Bers DM. The effect of temperature and ionic strength on the apparent ca-affinity of EGTA and the analogous ca-chelators BAPTA and dibromo-BAPTA. *Biochimica et Biophysica Acta (BBA)-General Subjects.* 1987; 925(2): 133-143.

30. Ha NT, Fujimori K, Henry PC, Tucker DJ. Assignment of 13C NMR chemical shift and microstructure of copolymers of 2-chloroethyl vinyl ether-maleic anhydride and n-butyl vinyl ether-maleic anhydride. *Polymer Bulletin.* 1999; 43(1): 81-85.

31. Wan F, Liu M, Zhang J, Li Y, Jiang L. Synthesis and characterization of DOTA-mono-adamantan-1-ylamide. *Research on Chemical Intermediates.* 2015; 41(8): 5109-5119.

32. Bellissent-Funel M. Water in biological systems: The NMR picture. *Hydration processes in biology: theoretical and experimental approaches.* 1999; 305: 233.

33. Edzes HT, Samulski ET. Cross relaxation and spin diffusion in the proton NMR of hydrated collagen. *Nature.* 1977; 265(5594): 521-523.

34. Zhang L, Wang L, Kao YT, Qiu W, Yang Y, Okobiah O, Zhong D. Mapping hydration dynamics around a protein surface. *Proc Natl Acad Sci U S A.* 2007 Nov 20; 104(47): 18461-18466. PMCID: PMC2141799.

35. Swift T, Swanson L, Geoghegan M, Rimmer S. The pH-responsive behaviour of poly (acrylic acid) in aqueous solution is dependent on molar mass. *Soft Matter.* 2016; 12(9): 2542-2549.

36. Jeong B, Gutowska A. Lessons from nature: Stimuli-responsive polymers and their biomedical applications. *Trends Biotechnol.* 2002; 20(7): 305-311.

37. Nelson A, Cosgrove T. Dynamic light scattering studies of poly (ethylene oxide) adsorbed on laponite: Layer conformation and its effect on particle stability. *Langmuir.* 2004; 20(24): 10382-10388.

38. Molnar RM, Bodnar M, Hartmann JF, Borbely J. Preparation and characterization of poly (acrylic acid)-based nanoparticles. *Colloid Polym Sci.* 2009; 287(6): 739-744.

39. Qu Z, Hu F, Chen K, Duan Z, Gu H, Xu H. A facile route to the synthesis of spherical poly (acrylic acid) brushes via RAFT polymerization for high-capacity protein immobilization. *J Colloid Interface Sci.* 2013; 398: 82-87.

40. Porsch B, Sundelöf L. Apparent aggregation behavior of poly (ethylene oxide) in water as a result of the presence of an impurity. *Macromolecules.* 1995; 28(21): 7165-7170.

41. Laguecir A, Ulrich S, Labille J, Fatin-Rouge N, Stoll S, Buffle J. Size and pH effect on electrical and conformational behavior of poly (acrylic acid): Simulation and experiment. *European polymer journal.* 2006; 42(5): 1135-1144.

42. Su Kim J, Ohk Kweon J, Tae Noh S. Online monitoring of reaction temperature during cationic ring opening polymerization of epichlorohydrin in presence of BF3 and 1, 4-butanediol. *J Appl Polym Sci.* 2014; 131(4).

43. Saddique FA, Zahoor AF, Faiz S, Naqvi SAR, Usman M, Ahmad M. Recent trends in ring opening of epoxides by amines as nucleophiles. *Synthetic Communications.* 2016; 46(10): 831-868.

44. Hyrc K, Bownik J, Goldberg M. Ionic selectivity of low-affinity ratiometric calcium indicators: Mag-fura-2, fura-2FF and BTC. *Cell Calcium.* 2000; 27(2): 75-86.

APPENDICES

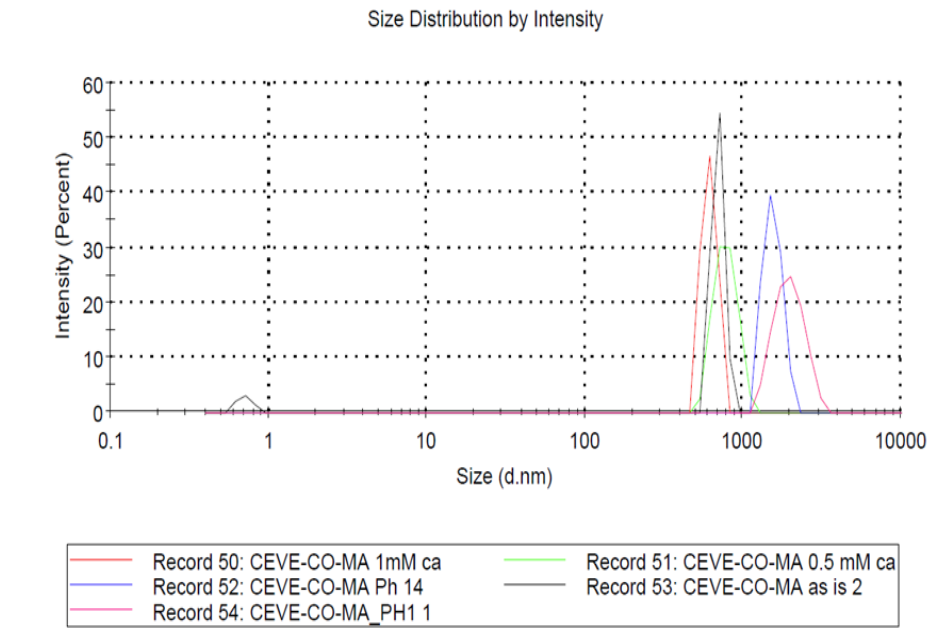

Appendix A.1- DLS size analysis in diameter of each sample modification

Appendix A.2- Set up of reaction for hydrogenation of n-BAPTA with hydrogen production reaction on the right and bubbling into reaction vessel on the left